Chapter 7
Two-body decay distributions beyond the dilepton case

Throughout the previous chapters we explored in detail the properties of the angular distribution of the dilepton decay of a vector particle. We will now illustrate a general method to calculate the shape of the angular distribution for any considered two-body decay, and survey examples for different kinds of initial particles, with integer or half-integer J.

We will focus on the following questions.

- How does the shape of the angular distribution depend on J and J_z? What are the observable parameters and their allowed physical values? How does the distribution depend on the identity of the decay products?
- If the nature of the decaying particle has not yet been identified and its angular momentum properties are unknown, how (and with what assumptions) can the measurement of the angular distribution lead to the determination of J?
- Apart from the previously discussed smearing effects in the indirect production from the decay of a $J = 0$ state, how can a $J > 0$ particle produce a completely isotropic two-body decay distribution, irrespectively of its polarization? Why is such an observation not a paradox?

P. Faccioli and C. Lourenço, *Particle Polarization in High Energy Physics*,
Lecture Notes in Physics 1002,
https://doi.org/10.1007/978-3-031-08876-6_7

7.1 Wigner rotation matrices

We saw in Chapter 1 how to calculate the dilepton decay angular distribution of a vector particle produced in a certain angular momentum configuration (its "polarization"), namely $|J, J_z\rangle = |1, 0\rangle_z$ or $|1, \pm 1\rangle_z$, or a superposition of these three cases, with respect to a given quantization axis z. In the following chapters we discussed in detail the properties of this distribution. In this chapter we consider several more decay distributions, involving initial and final particles of different categories, focusing on how they can be calculated in their general form and on how they reflect the angular momentum properties of the decaying particle.

The principal tool in all these calculations is the set of rotation transformations represented by the Wigner matrices [1]. Each matrix is identified by the value of the total angular momentum of the decaying particle, J. Its elements, $\mathcal{D}^J_{LL'}(\vartheta, \varphi)$, describe how an angular momentum state, with J_z projection L along a given axis z, transforms to a superposition of states of all possible projections L' along a different set of axes, rotated with respect to the original one by the spherical coordinates ϑ and φ. We introduced the Wigner matrices in Eq. 1.1 and defined them in Eq. 1.2, here reproduced for completeness:

$$\mathcal{D}^J_{LL'}(\vartheta, \varphi) = e^{-iL\varphi}\, d^J_{LL'}(\vartheta)\, e^{iL'\varphi}\,. \tag{7.1}$$

Before continuing with the description of these matrices, we will make a parenthesis to clarify that we use in this book a simpler notation than the one found in Refs. [2, 3] and other publications, where the rotation matrix elements are functions of the *three* Euler angles necessary to define a *completely generic* rotation in space, $D(\alpha, \beta, \gamma)$. That general transformation is the succession of a rotation around the z axis by the angle α, followed by a rotation around the (new) y axis by the angle β, and by a third rotation around, again, the (latest) z axis, this time by the angle γ, just as illustrated (except for the names of the angles) in Fig. 2.22, for the most generic change of reference frame.

In all calculations considered in this book, and in the general method used to calculate decay distributions, more examples of which will be seen in this chapter, the Wigner matrices are employed to rotate a *direction*, the one of the quantization axis, and not a three-dimensional shape; the number of angles parametrizing the rotation of a direction is two, not three, as would be needed to fully define the rotation of a generic three dimensional object with its own (not cylindrically symmetric) shape, like a generic wave function.

In fact, while the measurement of the decay angular distribution of a particle can be considered as a measurement of the particle's wave function, the wave functions of the decay products, which are the objects to which we apply the rotations in the calculation procedure, are not observed, unless they, in turn, decay *and* this further step is included as component of a higher-dimensional angular analysis.

Examples of the latter case are the cascade processes seen in Chapter 6, where the further decaying "daughter" (a J/ψ or Υ meson, or a Z boson) was represented by an additional Wigner matrix element changing the polarization axis of the dilepton

system as seen in the daughter's rest frame, therefore "giving life" to the daughter's three-dimensional nature and adding two more angles to the list of the observable degrees of freedom.

However, when the decay product is the "final" one, it has no associated "three-dimensional" structure that would justify the use of three angles for its rotation from a quantization "frame" to another: what we rotate in this case is only its quantization *axis* z and this operation depends only on the two angular coordinates defining the direction of the new axis with respect to the old axis.

To obtain this "minimal" rotation from the potentially more generic one described by the Wigner matrix, we have to impose that the two rotation components (first and third) around the z axis are the opposite of each other, i.e. $\gamma = -\alpha$. In this way, as can be recognized by observing the passages of the "cartoon" in Fig. 2.22 and inverting the direction of the last rotation step, the net effect is effectively a rotation made around the axis perpendicular to the plane containing the old and the new z axes, which is, in fact, the only meaningful option when no information exists about the shape of the rotated object. This is why we can use a simpler notation than the general one:

$$D^J_{LL'}(\varphi, \vartheta, -\varphi) \quad \rightarrow \quad \mathcal{D}^J_{LL'}(\vartheta, \varphi)\,. \tag{7.2}$$

It can now be observed that the complex exponential terms in Eq. 7.1 correspond to the two opposite rotations around the z axis (which, as explained in Section 2.15 and represented by Eq. 2.40, can be seen as shifts of the φ coordinate), while the ("reduced") d-matrix elements, $d^J_{LL'}(\vartheta)$, represent the polar-angle displacement from the z axis caused by the rotation around the y axis.

As already mentioned in Section 1.3, the reduced Wigner matrices can be computed with the expression

$$\begin{aligned} d^J_{LL'}(\vartheta) = & \sum_{t=\max(0,L-L')}^{\min(J+L,J-L')} (-1)^t \\ & \times \frac{\sqrt{(J+L)!\,(J-L)!\,(J+L')!\,(J-L')!}}{(J+L-t)!\,(J-L'-t)!\,t!\,(t-L+L')!} \\ & \times \left(\cos\frac{\vartheta}{2}\right)^{2J-(L'-L+2t)} \left(\sin\frac{\vartheta}{2}\right)^{L'-L+2t}. \end{aligned} \tag{7.3}$$

We alert the reader to the fact that two alternative conventions exist in the literature for this definition [1–4], only differing for a sign in certain configurations. They are entirely equivalent for the final physical results provided that, naturally, the same convention is systematically used in all the steps of the calculations. In this book we adopted and consistently used the convention of Ref. [2].

The number of computations can be significantly reduced through the use of the following relations (equivalent to Eq. 1.4):

$$\begin{aligned} d^J_{L,L'}(\vartheta) &= d^J_{-L',-L}(\vartheta)\,, \\ d^J_{L,L'}(\vartheta) &= (-1)^{L'-L}\, d^J_{L',L}(\vartheta)\,. \end{aligned} \tag{7.4}$$

The $d^J_{L,L'}(\vartheta)$ matrices are shown in Tables 7.1–7.6, respectively for $J = 1/2$, $3/2$, 1, 2, 3, and 4. In all tables we used two abbreviations, $c \equiv \cos(\vartheta/2)$ and $s \equiv \sin(\vartheta/2)$ (so that $c^2 + s^2 = 1$), to provide more compact expressions. It is worth noting that, since $0 < \vartheta < \pi$, both c and s are always positive. With this notation, $d^J_{J,J} = c^{2J}$ and $d^J_{-J,J} = s^{2J}$. As clearly seen in the definition of Eq. 7.3, all matrix elements are polynomials of order $2J$ in c and s.

Obviously, no table is needed for the $J = 0$ case, given that the only matrix element appearing in the formulas for its calculation, $d^0_{0,0}$, is independent of the

Table 7.1 The reduced Wigner matrix for the $J = 1/2$ case, $d^{1/2}_{L,L'}(\vartheta)$, with $c \equiv \cos(\vartheta/2)$ and $s \equiv \sin(\vartheta/2)$.

L	L'	
	$-1/2$	$+1/2$
$-1/2$	c	s
$+1/2$	$-s$	c

Table 7.2 The reduced Wigner matrix for the $J = 3/2$ case, $d^{3/2}_{L,L'}(\vartheta)$.

L	L'			
	$-3/2$	$-1/2$	$+1/2$	$+3/2$
$-3/2$	c^3	$\sqrt{3}\,c^2\,s$	$\sqrt{3}\,c\,s^2$	s^3
$-1/2$	$-\sqrt{3}\,c^2\,s$	$c\,(1-3s^2)$	$-(1-3c^2)\,s$	$\sqrt{3}\,c\,s^2$
$+1/2$	$\sqrt{3}\,c\,s^2$	$(1-3c^2)\,s$	$c\,(1-3s^2)$	$\sqrt{3}\,c^2\,s$
$+3/2$	$-s^3$	$\sqrt{3}\,c\,s^2$	$-\sqrt{3}\,c^2\,s$	c^3

Table 7.3 The reduced Wigner matrix for the $J = 1$ case, $d^1_{L,L'}(\vartheta)$.

L	L'		
	-1	0	$+1$
-1	c^2	$\sqrt{2}\,c\,s$	s^2
0	$-\sqrt{2}\,c\,s$	$2\,c^2-1$	$\sqrt{2}\,c\,s$
$+1$	s^2	$-\sqrt{2}\,c\,s$	c^2

Table 7.4 The reduced Wigner matrix for the $J = 2$ case, $d^2_{L,L'}(\vartheta)$.

L	L'				
	-2	-1	0	$+1$	$+2$
-2	c^4	$2\,c^3 s$	$\sqrt{6}\,c^2 s^2$	$2\,cs^3$	s^4
-1	$-2\,c^3 s$	$c^2\,(1-4\,s^2)$	$-\sqrt{6}\,cs\,(1-2\,c^2)$	$-(1-4\,c^2)\,s^2$	$2\,cs^3$
0	$\sqrt{6}\,c^2 s^2$	$\sqrt{6}\,cs\,(1-2\,c^2)$	$1-6\,c^2 s^2$	$-\sqrt{6}\,cs\,(1-2\,c^2)$	$\sqrt{6}\,c^2 s^2$
$+1$	$-2\,cs^3$	$-(1-4\,c^2)\,s^2$	$\sqrt{6}\,cs\,(1-2\,c^2)$	$c^2\,(1-4\,s^2)$	$2\,c^3 s$
$+2$	s^4	$-2\,cs^3$	$\sqrt{6}\,c^2 s^2$	$-2\,c^3 s$	c^4

Table 7.5 The reduced Wigner matrix for the $J = 3$ case, $d^3_{L,L'}(\vartheta)$.

L	L'						
	-3	-2	-1	0	$+1$	$+2$	$+3$
-3	c^6	$\sqrt{6}\,c^5 s$	$\sqrt{15}\,c^4 s^2$	$2\sqrt{5}\,c^3 s^3$	$\sqrt{15}\,c^2 s^4$	$\sqrt{6}\,cs^5$	s^6
-2	$-\sqrt{6}\,c^5 s$	c^4 $(1-6\,s^2)$	$\sqrt{10}\,c^3 s$ $(1-3\,s^2)$	$-\sqrt{30}\,c^2 s^2$ $(1-2\,c^2)$	$-\sqrt{10}\,cs^3$ $(1-3\,c^2)$	$-s^4$ $(1-6\,c^2)$	$\sqrt{6}\,cs^5$
-1	$\sqrt{15}\,c^4 s^2$	$-\sqrt{10}\,c^3 s$ $(1-3\,s^2)$	$c^2\,(1+5\,s^2$ $(1-3\,c^2))$	$2\sqrt{3}\,cs$ $(1-5\,c^2 s^2)$	$s^2\,(1+5\,c^2$ $(1-3\,s^2))$	$-\sqrt{10}\,cs^3$ $(1-3\,c^2)$	$\sqrt{15}\,c^2 s^4$
0	$-2\sqrt{5}\,c^3 s^3$	$-\sqrt{30}\,c^2 s^2$ $(1-2\,c^2)$	$-2\sqrt{3}\,cs$ $(1-5\,c^2 s^2)$	$-(1-2\,c^2)$ $(1-10\,c^2 s^2)$	$2\sqrt{3}\,cs$ $(1-5\,c^2 s^2)$	$-\sqrt{30}\,c^2 s^2$ $(1-2\,c^2)$	$2\sqrt{5}\,c^3 s^3$
$+1$	$\sqrt{15}\,c^2 s^4$	$\sqrt{10}\,cs^3$ $(1-3\,c^2)$	$s^2\,(1+5\,c^2$ $(1-3\,s^2))$	$-2\sqrt{3}\,cs$ $(1-5\,c^2 s^2)$	$c^2\,(1+5\,s^2$ $(1-3\,c^2))$	$\sqrt{10}\,c^3 s$ $(1-3\,s^2)$	$\sqrt{15}\,c^4 s^2$
$+2$	$-\sqrt{6}\,cs^5$	$-s^4$ $(1-6\,c^2)$	$\sqrt{10}\,cs^3$ $(1-3\,c^2)$	$-\sqrt{30}\,c^2 s^2$ $(1-2\,c^2)$	$-\sqrt{10}\,c^3 s$ $(1-3\,s^2)$	c^4 $(1-6\,s^2)$	$\sqrt{6}\,c^5 s$
$+3$	s^6	$-\sqrt{6}\,cs^5$	$\sqrt{15}\,c^2 s^4$	$-2\sqrt{5}\,c^3 s^3$	$\sqrt{15}\,c^4 s^2$	$-\sqrt{6}\,c^5 s$	c^6

polar and azimuthal decay angles, always resulting in an isotropic angular decay distribution.

To compare these compact expressions with those used in Chapter 1 and elsewhere, it is useful to keep in mind a few trigonometric identities, such as $\sin(\vartheta) = 2\cos(\vartheta/2)\sin(\vartheta/2)$, $\cos^2(\vartheta/2) = 1/2\,(1+\cos\vartheta)$, and $\sin^2(\vartheta/2) = 1/2\,(1-\cos\vartheta)$.

For visibility purposes, Table 7.6 is reported in truncated form, omitting the columns corresponding to $+1 \le L' \le +4$ and several of the terms in the displayed

Table 7.6 The reduced Wigner matrix for the $J = 4$ case, $d^4_{L,L'}(\vartheta)$. The missing matrix elements can be obtained using Eq. 7.4, as shown in the inset.

L \ L'	-4	-3	-2	-1	0
-4	c^8				
-3	$-2\sqrt{2}\,c^7 s$	$c^6(1-8s^2)$			
-2	$2\sqrt{7}\,c^6 s^2$	$-\sqrt{14}\,c^5 s(1-4s^2)$	$c^4(15-42c^2+28c^4)$		
-1	$-2\sqrt{14}\,c^5 s^3$	$\sqrt{7}\,c^4 s^2(3-8s^2)$	$-\sqrt{2}\,c^3 s(10-35c^2+28c^4)$	$c^2(-10+60c^2-105c^4+56c^6)$	
0	$\sqrt{70}\,c^4 s^4$	$2\sqrt{35}\,c^3 s^3(1-2c^2)$	$\sqrt{10}\,c^2(3-17c^2+28c^4-14c^6)$	$2\sqrt{5}\,cs(1-9c^2+21c^4-14c^6)$	$1-10\,c^2 s^2(2-7c^2+7c^4)$
$+1$	$-2\sqrt{14}\,c^3 s^5$	$-\sqrt{7}\,c^2 s^4(3-8c^2)$	$-\sqrt{2}\,cs^3(3-21c^2+28c^4)$	$-s^2(1-18c^2+63c^4-56c^6)$	
$+2$	$2\sqrt{7}\,c^2 s^6$	$\sqrt{14}\,cs^5(1-4c^2)$	$s^4(1-14c^2+28c^4)$		
$+3$	$-2\sqrt{2}\,cs^7$	$-s^6(1-8c^2)$			
$+4$	s^8				

L \ L'	-4	-3	-2	-1	0	$+1$	$+2$	$+3$	$+4$
-4	$\mathbf{d_{4,4}}$	$-d_{4,3}$	$d_{4,2}$	$-d_{4,1}$	$d_{4,0}$	$-d_{4,-1}$	$d_{4,-2}$	$-d_{4,-3}$	$d_{4,-4}$
-3	$\mathbf{d_{4,3}}$	$\mathbf{d_{3,3}}$	$-d_{3,2}$	$d_{3,1}$	$-d_{3,0}$	$d_{3,-1}$	$-d_{3,-2}$	$d_{3,-3}$	$-d_{4,-3}$
-2	$\mathbf{d_{4,2}}$	$\mathbf{d_{3,2}}$	$\mathbf{d_{2,2}}$	$-d_{2,1}$	$d_{2,0}$	$-d_{2,-1}$	$d_{2,-2}$	$-d_{3,-2}$	$d_{4,-2}$
-1	$\mathbf{d_{4,1}}$	$\mathbf{d_{3,1}}$	$\mathbf{d_{2,1}}$	$\mathbf{d_{1,1}}$	$-d_{1,0}$	$d_{1,-1}$	$-d_{2,-1}$	$d_{3,-1}$	$-d_{4,-1}$
0	$\mathbf{d_{4,0}}$	$\mathbf{d_{3,0}}$	$\mathbf{d_{2,0}}$	$\mathbf{d_{1,0}}$	$\mathbf{d_{0,0}}$	$-d_{1,0}$	$d_{2,0}$	$-d_{0,3}$	$d_{4,0}$
$+1$	$\mathbf{d_{4,-1}}$	$\mathbf{d_{3,-1}}$	$\mathbf{d_{2,-1}}$	$\mathbf{d_{1,-1}}$	$d_{1,0}$	$d_{1,1}$	$-d_{2,1}$	$d_{3,1}$	$-d_{4,1}$
$+2$	$\mathbf{d_{4,-2}}$	$\mathbf{d_{3,-2}}$	$\mathbf{d_{2,-2}}$	$d_{2,-1}$	$d_{2,0}$	$d_{2,1}$	$d_{2,2}$	$-d_{3,2}$	$d_{4,2}$
$+3$	$\mathbf{d_{4,-3}}$	$\mathbf{d_{3,-3}}$	$d_{3,-2}$	$d_{3,-1}$	$d_{3,0}$	$d_{3,1}$	$d_{3,2}$	$d_{3,3}$	$-d_{4,3}$
$+4$	$\mathbf{d_{4,-4}}$	$d_{4,-3}$	$d_{4,-2}$	$d_{4,-1}$	$d_{4,0}$	$d_{4,1}$	$d_{4,2}$	$d_{4,3}$	$d_{4,4}$

columns. The missing elements can be easily derived from those shown, using the symmetry relations presented in Eq. 7.4, as illustrated in the inset table.

7.2 Generic formulas for two-body decay distributions

To derive the shape of the dilepton decay distribution of the J/ψ, in Chapter 1, we used the following relevant physical constraints: a) the decaying particle has total angular momentum $J = 1$; b) the products are a fermion and an anti-fermion, of spin $1/2$ and mass negligible with respect to that of the mother particle; c) an intermediate vector boson (a virtual photon) couples to the final fermions preserving their helicities. These strong requirements effectively meant that we were considering a transition between two $J = 1$ (vector) systems, with the final one being "transversely polarized" ($J_{z'} = \pm 1$ along the common flight direction of the two fermions in the J/ψ rest frame). The resulting distributions and the meaning of their shape parameters were, obviously, specific to this well defined physical case.

We will now consider the *most general* case of two-body decays, $O \to X_1 X_2$, without any a priori constraint on the underlying physics. The result will depend on several amplitudes, in growing number with increasing values of the angular momentum quantum numbers of the initial (J) and final (J_1 and J_2) states. In this approach, physical hypotheses can be applied a posteriori, by restricting the possible number and values of the relevant amplitudes. Vice versa, an experimental measurement determining the observable shape parameters will put constraints on such amplitudes and, therefore, on the admissible hypotheses for the process being observed, sometimes even helping in the determination of the properties of the decaying particle.

For our completely generic description, we define a set of amplitudes, $\mathcal{A}_{M,G'_1,G'_2}$. As illustrated in Fig. 7.1-left, each coefficient represents the combined probability that O has angular momentum projection M along the chosen quantization axis z

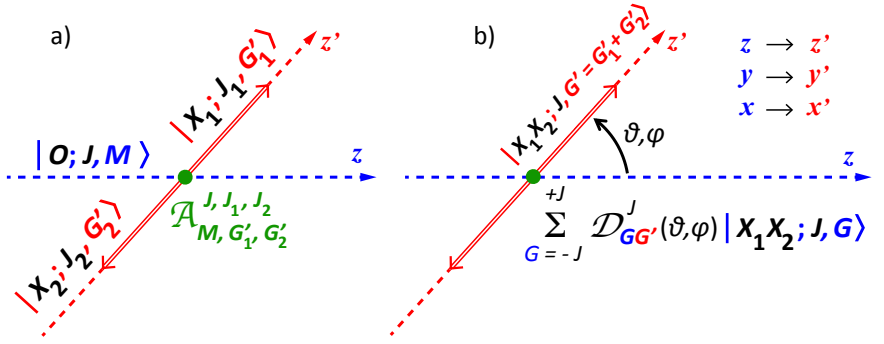

Fig. 7.1 Diagram of the $O \to X_1 X_2$ decay as seen in the O rest frame, specifying notations for axes, angles and angular momentum states of the initial and final particles.

(for example its momentum in the laboratory, that is the HX axis, or the direction of one or the other colliding beams, the two GJ axes, or the average of the two, the CS axis) and X_1 and X_2 have angular momentum projections G'_1 and G'_2 along the z' axis, defined by their common flight direction in the O rest frame (with a purely conventional orientation along the X_1 momentum).

We will consider the $\mathcal{A}_{M,G'_1,G'_2}$ amplitudes as generic complex numbers, without imposing any specific constraints. These are the coefficients that contain information on the underlying process dynamics, determining both the polarization state of O (the amplitudes a_M used in Chapter 1 are included in $\mathcal{A}_{M,G'_1,G'_2}$) and the angular momentum configurations of the decay products. They depend on the elementary couplings in the considered production and decay processes, which determine the allowed combinations of initial- and final-state "helicities" (angular momentum projections) and their probabilities. For example, in the decays of Standard Model vector gauge bosons (virtual photon, Z, W, gluon) into sufficiently light fermions, helicity conservation forbids terms with opposite fermion spin projections along z', so that $\mathcal{A}_{M,+1/2,-1/2} = \mathcal{A}_{M,-1/2,+1/2} = 0$. Moreover, considering for simplicity the leading-order process of Fig. 2.2-c, dominating towards low p_{T}, and choosing the CS frame, helicity conservation also forbids the J_z projection $M = 0$ for the initial state, that is, $\mathcal{A}_{0,G'_1,G'_2} = 0$.

We start by calculating the amplitude of the transition $O(M) \to X_1(G'_1)\, X_2(G'_2)$, which, by definition, involves the individual coefficient $\mathcal{A}_{M,G'_1,G'_2}$. Similarly to what we did in Chapter 1, and as illustrated in Fig. 7.1-right, we use the Wigner matrix to "project" the angular momentum state of the X_1X_2 system from the z' axis to the z axis:

$$|X_1X_2;\, J,\, G'_1 + G'_2\,\rangle_{z'} = \sum_{G=-J}^{+J} \mathcal{D}^{J}_{G,\,G'_1+G'_2}(\vartheta,\varphi)\; |X_1X_2;\, J,\, G\,\rangle_z\,. \tag{7.5}$$

Indicating with $\mathcal{B}_{M,G'_1,G'_2}$ the transition operator, the probability amplitude of the process can be written as

$$\begin{aligned}
\mathcal{A}\Big[O(M) \to X_1(G'_1)\, X_2(G'_2)\Big] \;&=\; {}_{z'}\langle X_1X_2;\, J,\, G'_1 + G'_2 \,|\, \mathcal{B}_{M,\,G'_1,G'_2} \,|\, O;\, J, M\rangle_z \\
&= \sum_{G=-J}^{+J} \mathcal{D}^{J*}_{G,\,G'_1+G'_2}(\vartheta,\varphi)\; {}_{z}\langle X_1X_2;\, J,\, G \,|\, \mathcal{B}_{M,\,G'_1,G'_2} \,|\, O;\, J, M\rangle_z \\
&= \sum_{G=-J}^{+J} \mathcal{D}^{J*}_{G,\,G'_1+G'_2}(\vartheta,\varphi)\; \delta_{M,G}\, \mathcal{A}_{M,\,G'_1,G'_2} \\
&= \mathcal{D}^{J*}_{M,\,G'_1+G'_2}(\vartheta,\varphi)\; \mathcal{A}_{M,\,G'_1,G'_2}\,,
\end{aligned} \tag{7.6}$$

where the relation ${}_{z}\langle X_1X_2;\, J,\, G \,|\, \mathcal{B}_{M,\,G'_1,G'_2} \,|\, O;\, J, M\rangle_z = \delta_{M,G}\, \mathcal{A}_{M,\,G'_1,G'_2}$ contains the conservation of J_z, in the Kronecker delta, and the process dynamics, in $\mathcal{A}_{M,G'_1,G'_2}$.

The following step in making the calculations more and more general consists in considering O to be produced not as a pure state having $J_z = M$, but as a superposition of J_z eigenstates; this is equivalent to taking the sum of all possible transition

amplitudes given by the previous equation:

$$\mathcal{A}\left[O \to X_1(G_1')\, X_2(G_2')\right] \;=\; \sum_{M=-J}^{+J} \mathcal{A}\left[O(M) \to X_1(G_1')\, X_2(G_2')\right] . \tag{7.7}$$

We note that, having defined $\mathcal{A}_{M,G_1',G_2'}$ to include the probability that O has J_z projection M, the sum does not contain the further coefficient a_M as it did, for example, in Eq. 1.10.

The square modulus of this amplitude gives the partial angular distribution for the specific angular momentum configurations G_1' and G_2' of the decay products:

$$\begin{aligned} &W_{G_1',G_2'}(\cos\vartheta,\varphi) = \\ &\sum_{|M|\le J,\,|N|\le J} \mathcal{A}^*\left[O(M) \to X_1(G_1')\, X_2(G_2')\right] \mathcal{A}\left[O(N) \to X_1(G_1')\, X_2(G_2')\right] \\ &= \sum_{|M|\le J,\,|N|\le J} \mathcal{D}^{J}_{M,\,G_1'+G_2'}(\vartheta,\varphi)\, \mathcal{D}^{J*}_{N,\,G_1'+G_2'}(\vartheta,\varphi)\, \mathcal{A}^*_{M,G_1',G_2'}\, \mathcal{A}_{N,G_1',G_2'} . \end{aligned} \tag{7.8}$$

As the final step, we sum over all allowed X_1 and X_2 angular momentum configurations (which are not observed, because eventual decay distributions of X_1 and X_2 are not part of the analysis):

$$W(\cos\vartheta,\varphi) \;=\; \sum_{\substack{|G_1'|\le J_1,\,|G_2'|\le J_2 \\ |G_1'+G_2'|\le \min\{J,\,J_1+J_2\}}} W_{G_1',G_2'}(\cos\vartheta,\varphi) . \tag{7.9}$$

The sum is made over all values of G_1' and G_2' satisfying angular momentum conservation. Besides the obvious relations $|G_1'| \le J_1$ and $|G_2'| \le J_2$, the inequality $|G_1' + G_2'| \le \min\{J,\, J_1 + J_2\}$ accounts for the fact that the relation $|J_1 - J_2| \le J \le J_1 + J_2$ is not necessarily satisfied when the decay products X_1 and X_2 have a relative orbital angular momentum $\mathbf{I_{1,2}}$, i.e. $\mathbf{J} = \mathbf{J_1} + \mathbf{J_2} + \mathbf{I_{1,2}}$. The presence of a nonzero $\mathbf{I_{1,2}}$ explains, for example, the existence of decays like $B^+ \to \mathrm{J}/\psi\, K^+$, where $J = 0$ and $|J_1 - J_2| = 1$, so that $J < |J_1 - J_2|$. In the next sections we will address several more cases, for example those where a particle of $J = 2$ decays to two spin-1/2 fermions, or a particle of $J = 1$ decays to two $J = 0$ particles, for which $J > J_1 + J_2$. When this latter condition happens, $|G_1' + G_2'|$ never reaches the value J, because the orbital angular momentum $\mathbf{I_{1,2}}$ has always projection zero along the quantization axis of the decay products (z') and does not contribute to a possible larger magnitude of $G_1' + G_2'$.

The dependence of the distribution on the dynamical amplitudes $\mathcal{A}_{M,G_1',G_2'}$ is usually reorganized into a set of complex coefficients,

$$\rho^{G'}_{M,N} \;=\; \sum_{\substack{|G_1'|\,\le\, J_1,\,|G_2'|\,\le\, J_2 \\ G_1'+G_2'=G'}} \mathcal{A}^*_{M,G_1',G_2'}\, \mathcal{A}_{N,G_1',G_2'} , \tag{7.10}$$

which form, for each G', the so-called "spin density matrix", a hermitian matrix ($\rho^{G'}_{M,N} = \rho^{G'*}_{N,M}$) with trace

$$\sum_{\substack{|G'_1| \le J_1,\, |G'_2| \le J_2 \\ G'_1+G'_2=G',\, |M| \le J}} \left|\mathcal{A}_{M,G'_1,G'_2}\right|^2 = 1\,. \tag{7.11}$$

Therefore, the angular distribution is written, combining Eqs. 7.8, 7.9 and 7.10, as

$$\begin{aligned} W(\cos\vartheta,\varphi) &= \sum_{\substack{|G'| \le \min(J,J_1+J_2) \\ |M| \le J,\, |N| \le J}} \rho^{G'}_{M,N}\; \mathcal{D}^{J}_{M,G'}(\vartheta,\varphi)\, \mathcal{D}^{J*}_{N,G'}(\vartheta,\varphi) \\ &= \sum_{\substack{|G'| \le \min(J,J_1+J_2) \\ |M| \le J,\, |N| \le J}} \rho^{G'}_{M,N}\; d^{J}_{M,G'}(\cos\vartheta)\, d^{J}_{N,G'}(\cos\vartheta)\, e^{-i\,(M-N)\,\varphi}\,. \end{aligned} \tag{7.12}$$

The ultimate generalization consists in considering the sum over all possible subprocesses contributing to the production of O, with weights proportional to their relative yields. For this purpose it is sufficient to define the corresponding weighted average of the density matrix,

$$\rho^{G'}_{M,N} = \sum_{\substack{|G'_1| \le J_1,\, |G'_2| \le J_2 \\ G'_1+G'_2=G'}} \left\langle \mathcal{A}^{*}_{M,G'_1,G'_2}\; \mathcal{A}_{N,G'_1,G'_2} \right\rangle\,, \tag{7.13}$$

while the final expression of the angular distribution remains formally the one of Eq. 7.12.

A note of caution is due about the possibly misleading notation used for the dynamical amplitudes $\mathcal{A}_{M,G'_1,G'_2}$ and for the spin density matrix elements $\rho^{G'}_{M,N}$. These objects appear in expressions like Eqs. 7.8 and 7.12, where we see them together with Wigner matrix elements, which are the only ones explicitly having "J" as index. However, they actually depend on all the details of the production and decay dynamics and, in particular, on J, J_1, and J_2, despite the fact that these symbols are not explicitly shown as indices.

7.3 The polar projection of the decay distribution

There are cases where only the polar angle dependence of the decay distribution is effectively interesting for the study of the process under consideration. The azimuthal dependence of the distribution obviously vanishes when the particle is produced in $2 \to 1$ processes and the polarization axis z is chosen along the only meaningful direction, that of the relative momentum of the colliding particles (CS frame). The same happens along any other polarization axis if the particle is produced in a single, pure J_z eigenstate along that direction. For these cases, it is convenient to

consider directly the generic expression of the $\cos\vartheta$ distribution, as obtained by averaging Eq. 7.12 over φ. Given that the azimuthal dependence is exclusively contained in the complex exponential factor of that expression, and that

$$\frac{1}{2\pi}\int_{-\pi}^{+\pi} e^{-i\,(M-N)\,\varphi}\; d\varphi = \delta_{M,N}\;, \tag{7.14}$$

the resulting averaged distribution is

$$w(\cos\vartheta) \;=\; \sum_{\substack{|G'|\leq \min(J,J_1+J_2)\\ |M|\leq J}} \sigma_M^{G'}\left[d^J_{M,G'}(\cos\vartheta)\right]^2\;, \tag{7.15}$$

which only depends on the squared moduli of the helicity amplitudes, that is, on the "diagonal" (and real) $\rho^{G'}_{M,M}$ terms:

$$\sigma_M^{G'} \;\equiv\; \rho^{G'}_{M,M} \;=\; \sum_{\substack{|G'_1|\,\leq\, J_1,\; |G'_2|\,\leq\, J_2\\ G'_1+G'_2\,=\,G'}} \left\langle \left|\mathcal{A}_{M,G'_1,G'_2}\right|^2 \right\rangle\,. \tag{7.16}$$

As can be seen in Tables 7.1–7.6, the square of any reduced d-matrix element is, for all cases of J, both integer and half-integer, a linear combination of terms of the kind $\sin^Q(\vartheta/2)\,\cos^P(\vartheta/2)$ with *even* Q and P values, that is, of terms of the kind $(1-\cos\vartheta)^{Q/2}\,(1+\cos\vartheta)^{P/2}$. The maximum overall power $Q+P$ in each d^2 expression is $4J$. Therefore, the polar angle distribution will be a polynomial of order $2J$ in $\cos\vartheta$, with $2J$ independent observable coefficients, λ_i,

$$w(\cos\vartheta \mid \boldsymbol{\lambda}) \;=\; \frac{1}{\mathcal{N}}\left[\,1+\sum_{i=1}^{2J}\lambda_i\,(\cos\vartheta)^i\,\right], \tag{7.17}$$

where the normalization $\mathcal{N}$ is equal to $1+\sum\lambda_j\,/\,(j+1)$, with the sum being made only over the *even* natural numbers $j\leq 2J$. The terms with odd powers of $\cos\vartheta$ are parity violating.

We should keep in mind that any information about the interference between the different angular momentum eigenstates composing the initial state is lost in the polar projection of the distribution. The decaying particle can be a coherent or an incoherent superposition of eigenstates. As seen in Chapter 1, these two physically different cases lead to different azimuthal anisotropies, properly reflected in Eq. 7.12, but not to different polar anisotropies, thereby being indistinguishable in the polar projection. As has been discussed a number of times in this book, *neglecting* the possible existence of significant azimuthal anisotropies can create problems, both for the accuracy of the measurement and for the interpretation of the results.

On the other hand, as we study cases of increasing J, the simplification of considering only the $\cos\vartheta$ dimension becomes more and more convenient. For $J=1$, in the most general case, including parity-violating effects, the maximum number of observable parameters of the full distribution is eight (five of them potentially non-

negligible if the particle is observed inclusively, without referring the polarization axes to possible accompanying particles in the event), while the polar projection only has two measurable parameters, clearly allowing for a substantial simplification of the analysis procedure.

In the $J = 2$ case, the total number of parameters increases from 8 to 24, their measurement requiring very challenging procedures, and even in the simpler option of inclusive observation we still need to consider 14 "significant parameters". Instead, when only considering the $\cos\vartheta$ distribution, the number of parameters drops to four, vastly reducing the complexity of the experimental analysis.

7.4 The general $J = 1$ two-body decay distribution

In the derivation of the decay distribution of a vector particle into two leptons, in Chapter 1, we have used the physical constraint of helicity conservation, which imposes that the final dilepton has projection $G' = G'_1 + G'_2 = \pm 1$ along the decay direction in the mother's rest frame. By removing this constraint we can obtain, using Eq. 7.12, the most general two-body decay distribution of any $J = 1$ state. Its parametrization is formally unchanged with respect to the dilepton case (Eq. 1.29):

$$\begin{aligned} W(\cos\vartheta,\varphi) \;=\; & \frac{3}{4\pi}\frac{1}{(3+\lambda_\vartheta)}\,(1+\lambda_\vartheta\cos^2\vartheta \\ & + \lambda_\varphi \sin^2\vartheta\cos 2\varphi + \lambda_{\vartheta\varphi}\sin 2\vartheta\cos\varphi \\ & + \lambda^{\perp}_{\varphi}\sin^2\vartheta\sin 2\varphi + \lambda^{\perp}_{\vartheta\varphi}\sin 2\vartheta\sin\varphi \\ & + 2A_\vartheta\cos\vartheta + 2A_\varphi\sin\vartheta\cos\varphi + 2A^{\perp}_{\varphi}\sin\vartheta\sin\varphi)\,. \end{aligned} \tag{7.18}$$

Compared to those of Eq. 1.28, however, the shape parameters have now the additional dependence on the $G' = 0$ amplitudes (through the elements $\rho^0_{M,N}$ of the spin density matrix):

$$\begin{aligned} \lambda_\vartheta \;&=\; 1/D\,\Big[\rho^{+1}_{+1,+1} + \rho^{-1}_{+1,+1} - 2\rho^{0}_{+1,+1} + \rho^{+1}_{-1,-1} + \rho^{-1}_{-1,-1} - 2\rho^{0}_{-1,-1} \\ &\qquad - 2\left(\rho^{+1}_{0,0} + \rho^{-1}_{0,0} - 2\rho^{0}_{0,0}\right)\Big], \\ \lambda_\varphi \;&=\; 2/D\,\mathrm{Re}\left(\rho^{+1}_{+1,-1} + \rho^{-1}_{+1,-1} - 2\rho^{0}_{+1,-1}\right), \\ \lambda^{\perp}_{\varphi} \;&=\; 2/D\,\mathrm{Im}\left(\rho^{+1}_{+1,-1} + \rho^{-1}_{+1,-1} - 2\rho^{0}_{+1,-1}\right), \\ \lambda_{\vartheta\varphi} \;&=\; \sqrt{2}/D\,\mathrm{Re}\left[\rho^{+1}_{+1,0} + \rho^{-1}_{+1,0} - 2\rho^{0}_{+1,0} - \left(\rho^{+1}_{0,-1} + \rho^{-1}_{0,-1} - 2\rho^{0}_{0,-1}\right)\right], \\ \lambda^{\perp}_{\vartheta\varphi} \;&=\; \sqrt{2}/D\,\mathrm{Im}\left[\rho^{+1}_{+1,0} + \rho^{-1}_{+1,0} - 2\rho^{0}_{+1,0} - \left(\rho^{+1}_{0,-1} + \rho^{-1}_{0,-1} - 2\rho^{0}_{0,-1}\right)\right], \end{aligned} \tag{7.19}$$

$$A_\vartheta = 1/D \left(\rho^{+1}_{+1,+1} - \rho^{-1}_{+1,+1} + \rho^{-1}_{-1,-1} - \rho^{+1}_{-1,-1}\right),$$

$$A_\varphi = \sqrt{2}/D \,\mathrm{Re}\left(\rho^{+1}_{+1,0} - \rho^{-1}_{+1,0} + \rho^{+1}_{0,-1} - \rho^{-1}_{0,-1}\right),$$

$$A^\perp_\varphi = \sqrt{2}/D \,\mathrm{Im}\left(\rho^{+1}_{+1,0} - \rho^{-1}_{+1,0} + \rho^{+1}_{0,-1} - \rho^{-1}_{0,-1}\right),$$

where the denominator is

$$D = \rho^{+1}_{+1,+1} + \rho^{-1}_{+1,+1} + 2\,\rho^{0}_{+1,+1} + \rho^{+1}_{-1,-1} + \rho^{-1}_{-1,-1} + 2\,\rho^{0}_{-1,-1} + 2\left(\rho^{+1}_{0,0} + \rho^{-1}_{0,0}\right).$$

The parameters transform from one reference frame to another exactly as in the dilepton case (Section 2.15). Their physically allowed domain is shown in Fig. 7.2, where its two-dimensional projections are represented by the blue areas. Superimposed to these are, in gold, the corresponding projections (reproduced from Fig. 3.4) for the dilepton (or light quark-antiquark) decay via intermediate vector boson, illustrating how the additional requirement of helicity conservation ($\rho^0_{M,N} = 0$) restricts the parameter domain. We also remind that the same constraint is present in the decays to a $J = 0$ particle accompanied by a real photon; for example, the decays $\rho^0 \to \ell^+\ell^-$ and $\rho^0 \to \pi^0\gamma$ have identical angular distributions.

Frame-independent polarization parameters exist and are formally defined, as functions of the λ and A parameters, exactly as those of the dilepton distribution (Chapter 3), even if their meaning in terms of natural polarizations can be different.

This generalized $J = 1$ decay distribution can be used to describe many physical decays beyond the dilepton case, such as, for instance, $\mathrm{Z} \to \mathrm{J}/\psi\,\gamma$, the radiative transitions of $J = 1$ mesons, like $\chi_{c1} \to \mathrm{J}/\psi\,\gamma$ or $\psi(2\mathrm{S}) \to \chi_{cJ}\,\gamma$ (with $J = 0, 1, 2$), and several hadronic decays [5].

As an illustration, we will calculate the polar anisotropy parameter of the decays $\chi_{c1} \to \mathrm{J}/\psi\,\gamma$ and $\mathrm{Z} \to \mathrm{J}/\psi\,\gamma$ (and the equivalent ones with the charmonium states replaced by the corresponding bottomonium ones). The decaying particle is the generic combination $|\,O\,\rangle = \sum_{M=-1}^{+1} a_M\ |1,\ M\,\rangle$. As done in Section 6.7 to calculate the J/ψ decay anisotropy, we refer to the axis z' (Fig. 6.32), along which the J/ψ and the γ have back-to-back momenta in the mother's rest frame, and to the coefficients listed in Table 6.2, expressing the relative probabilities of the configurations with specific $J_{z'}$ projections of J/ψ and γ. This time, the method is applied to calculate the anisotropy of the χ_{c1} or Z two-body decay.

Considering the column $J = 1$ of Table 6.2 and keeping only the lines with $K' = \pm 1$ (transversely polarized photon), we see that there are two allowed configurations with $G' = L' + K' = 0$, having total weight $1/2 + 1/2 = 1$, while the cases $G' = +1$ and $G' = -1$ only have one configuration each, with weight $1/2$. The J/$\psi\,\gamma$ state is then "polarized", because the three cases, $G' = -1$, 0 and $+1$, have unequal weights: as will be discussed in Section 7.8, this is a condition for the observability of the polarization of the mother particle. The diagonal spin densities (i.e. the squared amplitudes) $\sigma^{G'}_M = \rho^{G'}_{M,M}$ are proportional to those weights, times the probability $|a_M|^2$ that the decaying state $|\,O\,\rangle$ has $J_z = M$:

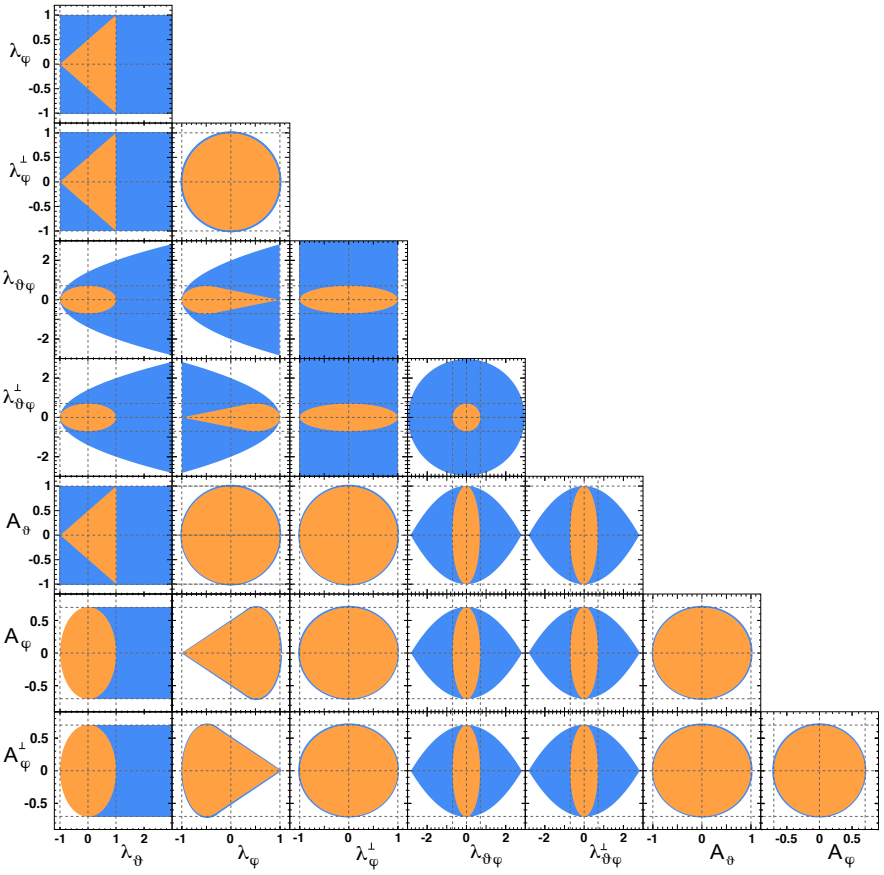

Fig. 7.2 Allowed parameter regions of the two-body decay distribution of a $J = 1$ particle. The largest areas (blue) represent the most general domain while the inner areas (gold) represent the dilepton decay case. In the most general case there are no upper bounds on λ_ϑ and $|\lambda_{\vartheta\varphi}|$, but the bound $\lambda_\vartheta < 3$ was added to enable the graphical representation.

$$\sigma_M^{+1} = \sigma_M^{-1} \propto \frac{1}{2}|a_M|^2\,, \quad \sigma_M^0 \propto |a_M|^2\,. \tag{7.20}$$

Substituted in Eq. 7.19, with the normalization $|a_{-1}|^2 + |a_0|^2 + |a_{+1}|^2 = 1$, these give

$$\lambda_\vartheta = -\frac{1 - 3\,|a_0|^2}{3 - |a_0|^2}\,. \tag{7.21}$$

This is the polar anisotropy of the J/ψ (or photon) emission direction in the χ_{c1} rest frame, equal (as already seen in Section 6.6) to $-1/3$, 0 and $+1$ when, respectively, $|a_0|^2 = 0$, $1/3$ and 1, while values of λ_ϑ smaller than $-1/3$ or larger than $+1$ are forbidden. Repeating the exercise for the decay where the emitted photon is virtual (as in the case $\chi_{c1} \to \mathrm{J}/\psi\,\gamma^*$), this time including in the count, therefore,

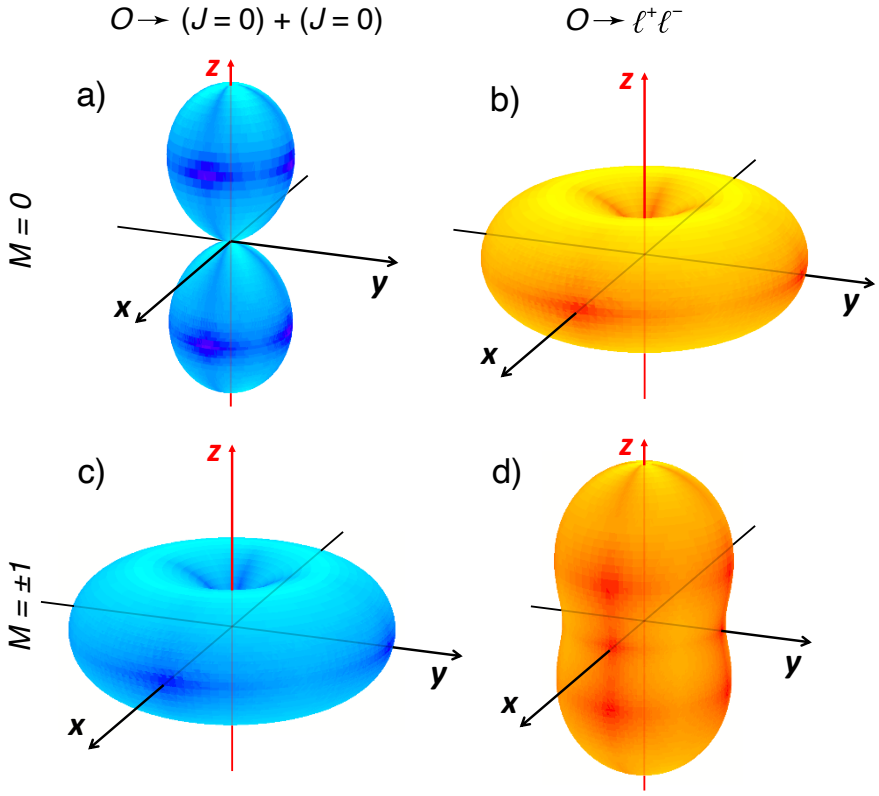

Fig. 7.3 A longitudinally (top panels) or transversely (bottom panels) polarized vector particle O produces two different decay angular distributions when it decays into a $J = 0$ meson and its antimeson (left panels) or into a lepton-antilepton pair (right panels).

the $K' = 0$ term, we can see that now the three cases, $G' = -1$, 0 and $+1$, are equiprobable and, for any M, the anisotropy parameters are zero: the J/ψ is emitted isotropically in the χ_c rest frame, independently of the χ_c polarization. This confirms the result found, with a different method, in Section 6.8.

It is interesting to consider the case where the two final particles have both spin $J = 0$, illustrated by the left drawings of Fig. 7.3. This example is "complementary" to the dilepton one (shown in the right drawings of the same figure): the $J_{z'}$ projection $G' = 0$ of the final system is not only allowed, but is now the *only* physical possibility, given that the relative orbital component $I = 1$, required by angular momentum conservation, has zero projection along the common direction of two back-to-back products. The maximum allowed domain is not different from the general case shown in blue in Fig. 7.2, except that the parity-violating asymmetries A_ϑ, A_φ, and $A_\varphi^\perp$ must always vanish, for the same reason why A_ϑ can only be zero when the *initial* state has zero J_z projection (Sections 1.3 and 1.4): the squared matrix element $(d^1_{M,0})^2$, just like $(d^1_{0,G'})^2$, is a function of only the parity conserving expres-

sion $\cos^2\vartheta$ (Table 7.3). Relevant physical cases include, for example, the decays $\rho(770)^{\pm,0} \to \pi^{\pm}\pi^0$ / $\pi^+\pi^-$, $\phi(1020) \to K^+K^-$, and $\Upsilon(4S) \to B\overline{B}$ [5].

The particles $\rho(770)$, $\phi(1020)$, and $\Upsilon(4S)$ also decay to dileptons and it is interesting to compare the shapes of the angular distributions of two decay channels. The decay into a pair of $J = 0$ mesons gives an interesting illustration of the seemingly strange fact that, as seen in Fig. 7.2, λ_ϑ (and therefore $|\lambda_{\vartheta\varphi}|$) can assume values larger than +1. Actually, λ_ϑ even tends to $+\infty$ when the spin density matrix element $\rho^0_{0,0}$ dominates over all others, given that, as seen in Eq. 7.19, it is the only element not appearing in the denominator (or constant factor) D, which therefore tends to vanish. This limit corresponds to the hypothetical case when the vector particle $\rho(770)$, $\phi(1020)$, or $\Upsilon(4S)$ is produced *longitudinally* polarized ($M = 0$) in the chosen frame. Equations 7.18 and 7.19 are then simply replaced by

$$W(\cos\vartheta, \varphi) \;=\; \frac{3}{4\pi}\,\cos^2\vartheta\,, \tag{7.22}$$

a shape very different from the one of the dilepton decay distribution (where, for any λ_ϑ, a significant fraction of events is emitted at around $\cos\vartheta = 0$) and in particular, as shown in Fig. 7.3-a, from the one of the dilepton decay of a longitudinally polarized vector particle, which is $\propto 1 - \cos^2\vartheta$ (Fig. 7.3-b).

In the case of transverse polarization the roles are inverted: in the di-meson decay, when only the $\rho^0_{M,N}$ matrix elements with $M, N = \pm 1$ are nonzero λ_ϑ assumes the maximum possible negative value, -1 (Fig. 7.3-c), while $\lambda_\vartheta = +1$ in the dilepton decay, where the nonzero elements are $\rho^{\pm 1}_{M,N}$ (Fig. 7.3-d). For example, the $\Upsilon(4S)$ resonance is produced transversely polarized in e^+e^- colliders because of helicity conservation in the coupling between the colliding leptons and the intermediate virtual photon; Fig. 7.3-c represents, therefore, the distribution of the emission directions of the B and $\overline{B}$ mesons with respect to the direction, z, of the beams.

A further example leading to this distribution shape is represented by the decays of ρ and ϕ mesons to pion or kaon pairs, when the ρ and ϕ are produced (always transversely polarized) in the radiative decays $H \to \rho\gamma$ or $H \to \phi\gamma$; in this case the natural axis with respect to which $\lambda_\vartheta = -1$ is the meson direction in the H rest frame (cHX frame).

7.5 Polar anisotropy of the $J = 2$ two-body decay distribution

Expanding Eq. 7.15 and reordering the result according to Eq. 7.17, we obtain the polar projection of the two-body decay distribution of a $J = 2$ particle, described by four independent parameters:

$$\lambda_1 = 4\,(\beta_{22} - 2\beta_{11} + 4\beta_{12})\,/\,D\,,$$

$$\lambda_2 = 6\,(\alpha_{22} - \alpha_{00} - 2\,\alpha_{02} - 2\,\alpha_{11} + 4\,\alpha_{01})\,/\,D\,,$$

$$\lambda_3 = 4\,(\beta_{22} + 4\beta_{11} - 4\beta_{12})\,/\,D\,, \tag{7.23}$$

$$\lambda_4 = (\alpha_{22} + 9\,\alpha_{00} + 6\,\alpha_{02} + 16\,\alpha_{11} - 24\,\alpha_{01} - 8\,\alpha_{12})\,/\,D\,,$$

$$\text{with}\;\; D = \alpha_{22} + \alpha_{00} + 6\,\alpha_{02} + 4\,\alpha_{11} + 8\,\alpha_{12}\,,$$

and

$$\begin{aligned} \alpha_{i,j} &= \sigma_i^j + \sigma_j^i + \sigma_{-i}^{-j} + \sigma_{-j}^{-i} + \sigma_i^{-j} + \sigma_{-j}^i + \sigma_{-i}^j + \sigma_j^{-i} \\ \beta_{i,j} &= \sigma_i^j + \sigma_j^i + \sigma_{-i}^{-j} + \sigma_{-j}^{-i} - \left(\sigma_i^{-j} + \sigma_{-j}^i + \sigma_{-i}^j + \sigma_j^{-i}\right). \end{aligned} \tag{7.24}$$

Given the, respectively, symmetric and antisymmetric definitions of $\alpha_{i,j}$ and $\beta_{i,j}$ by exchange between initial- and final-state helicities, λ_2 and λ_4 are parity-conserving, while λ_1 and λ_3 are parity-violating.

As a simple application of these relations, along the line of the previous section, where we considered the radiative χ_{c1} or Z decays to J/ψ, we examine here the analogous decay $\chi_{c2} \to \mathrm{J}/\psi\,\gamma$, where now $|\chi_{c2}\rangle = \sum_{M=-2}^{+2} a_M\,|2,\,M\rangle$. The relevant weights in Table 6.2 are 1, 1, 1/2, 1/2, and 1/6 + 1/6 = 1/3, respectively for the J/$\psi\,\gamma$ configurations $G' = L' + K' = +2, -2, +1, -1$, and 0. Therefore,

$$\sigma_M^{+2} = \sigma_M^{-2} \propto |a_M|^2\,, \quad \sigma_M^{+1} = \sigma_M^{-1} \propto \frac{1}{2}\,|a_M|^2\,, \quad \sigma_M^0 \propto \frac{1}{3}\,|a_M|^2\,, \tag{7.25}$$

and Eq. 7.23 gives, after some algebra, the polar anisotropy of the J/ψ emission in the χ_{c2} rest frame:

$$\lambda_2 = \frac{3\left[\,2\left(|a_{+2}|^2\,|a_{-2}|^2\right) - \left(|a_{+1}|^2\,|a_{-1}|^2\right) - 2\,|a_0|^2\,\right]}{6\left(|a_{+2}|^2\,|a_{-2}|^2\right) + 9\left(|a_{+1}|^2\,|a_{-1}|^2\right) + 10\,|a_0|^2}\,, \tag{7.26}$$

$$\lambda_1 = \lambda_3 = \lambda_4 = 0\,.$$

The parameter λ_2 has values between $-3/5$ and $+1$, being equal to $-3/5$, $-1/3$, and $+1$ when the χ_{c2} is produced with the respective J_z projections $M = 0, \pm 1$, and ± 2, as already found in Section 6.6. When the emitted photon is virtual ($\chi_{c2} \to \mathrm{J}/\psi\,\gamma^*$) and the cases with $K' = 0$ are allowed, the same procedure leads to the fully isotropic and polarization-independent result $\lambda_1 = \lambda_2 = \lambda_3 = \lambda_4 = 0$, as in the χ_{c1} case and as already found in Section 6.8.

The physical domain of parameter space depends on the type of decay products and on the production mechanism; some examples are shown in Figs. 7.4 and 7.5. The grey contours in both figures represent the allowed regions including all possible physical cases: they reflect only angular momentum conservation and rotation invariance, which shape the general dependences of the parameters λ_i on the different process amplitudes, as described by Eq. 7.23. The more restricted, coloured areas represent specific physics hypotheses.

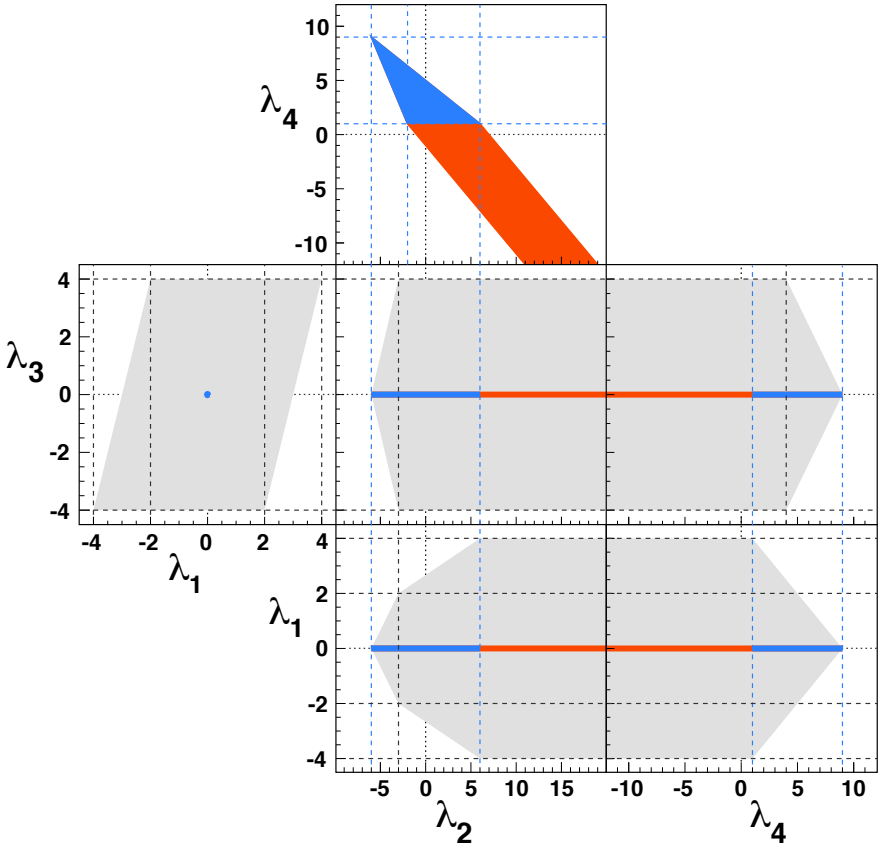

Fig. 7.4 Allowed parameter regions of the polar projection of the two-body decay distribution of a $J = 2$ particle O. The largest areas (grey) represent the most general domain. The intermediate areas (red+blue) represent any of two equivalent cases: O decays into two real photons; O is produced alone from the scattering of two real gluons (and the measurement is made in the CS frame). The smallest areas (blue) represent the case where both hypotheses are satisfied. There is no upper bound on λ_2 and no lower bound on λ_4.

The union of the blue and red areas in Fig. 7.4 corresponds to the case where the decay products are two real photons, a condition translating into $\sigma_M^{\pm 1} = 0$ for any M, given that $G' = \pm 1$ would mean that one of the two photons is not transversely polarized. Known $J = 2$ particles seen in the photon-photon channel are, for example, $a_2(1320)$, $a_2(1700)$, $\eta_2(1870)$, and $X(3915)$, the latter with spin assignment still uncertain between $J = 0$ and $J = 2$ [5].

Given the symmetry of the equations in Eq. 7.23, in particular the properties of $\alpha_{i,j}$ and $\beta_{i,j}$ (Eq. 7.24) by exchange of the i and j indices, identical contours (blue plus red) are obtained by reversing the role of initial and final states, forbidding this time that the decaying particle is produced in the $M = \pm 1$ state ($\sigma_{\pm 1}^{G'} = 0$ for any G'). This corresponds, for example, to the production via scattering of two real gluons

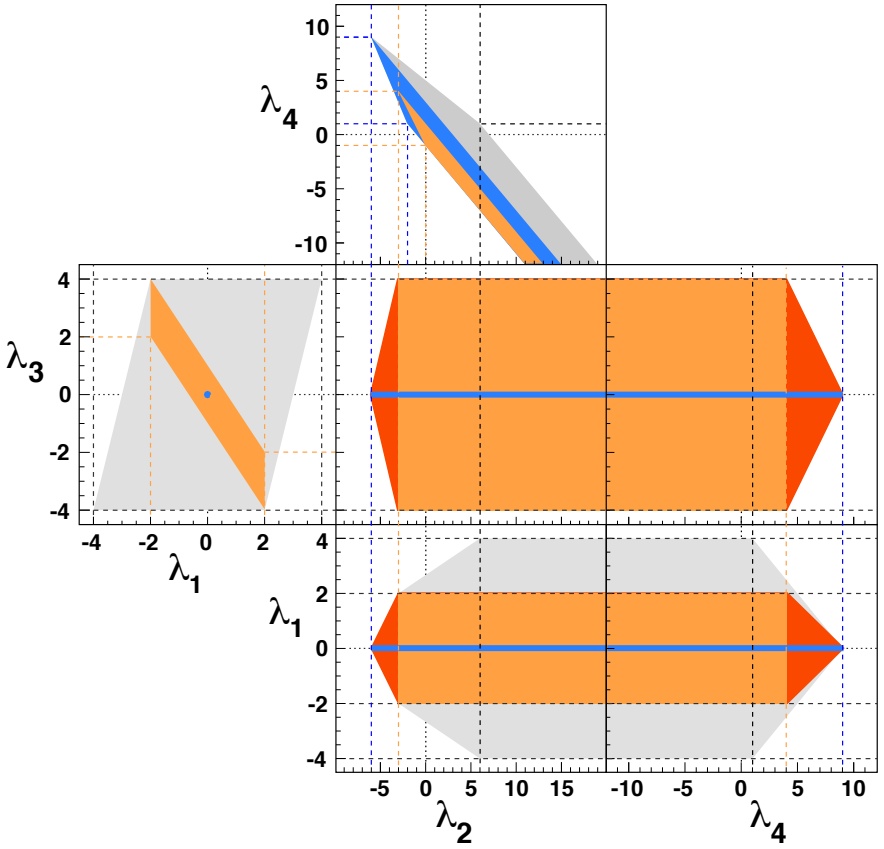

Fig. 7.5 Allowed parameter regions of the polar projection of the two-body decay distribution of a $J = 2$ particle O. The largest areas (grey) represent the most general domain. The intermediate areas (red+blue+orange) represent the case in which O decays into two $J = 1/2$ fermions. The blue areas correspond to the hypothesis that O is produced alone from the scattering of two real gluons *and* decays into two $J = 1/2$ fermions, for measurements made in the CS frame; alternatively, they describe the decay into two $J = 0$ particles. The orange areas refer to the $G' = \pm 1$ case, for example a decay into $J = 0$ particle plus photon. There is no upper bound on λ_2 and no lower bound on λ_4.

in $2 \to 1$ processes (that is, with no recoiling particle); in this case, however, the contours refer only to a measurement where the polarization axis is chosen along the scattering direction of the gluons (CS frame).

When either the elementary production process is initiated by two identical particles or the decay products are two identical particles, the parity-violating terms λ_1 and λ_3 obviously vanish, resulting in simple lines or dots as allowed regions in the two-dimensional projected domains. The smallest, blue areas show the case when *both* of these hypotheses apply: the particle is produced in gluon-gluon fusion and decays into two photons.

This intersection is particularly interesting in the search for unknown boson resonances of mass, m, higher than the mass of any known particle, as discussed in the next section; in fact, such objects would be observed in the domain of very low p_T/m values, where the presence of a recoiling particle is not necessary nor probable. The di-photon decay represented, for example, the discovery channel of the Higgs boson.

Hypotheses on the properties of the fundamental couplings involved can, obviously, further restrict the allowed regions or even fix the values of the λ_i parameters. For example, considering the gluon-gluon to photon-photon case (where $\lambda_1 = \lambda_3 = 0$), the hypothesis of a graviton-like $J = 2$ particle interacting with SM bosons with no helicity flip [6] (corresponding to the *additional* conditions $\sigma_0^{G'} = \sigma_M^0 = 0$ for any G' and M: overall, only $G' = \pm 2$ and $M = \pm 2$ are allowed) leads to $\lambda_2 = 6$ and $\lambda_4 = 1$, the rightmost vertex of the blue triangle in the λ_2–λ_4 plane.

Further examples are shown in Fig. 7.5. Here the intermediate areas, in colour (union of blue, red, and orange), represent the case in which the particle decays into two $J = 1/2$ fermions, but with no assumption of helicity conservation, therefore only forbidding the $G' = \pm 2$ projection: $\sigma_M^{\pm 2} = 0$.

The blue areas (blue plus orange in the λ_4 vs. λ_2 case) are obtained by, additionally, imposing that also the $G' = \pm 1$ component is absent, $\sigma_M^{\pm 1} = \sigma_M^{\pm 2} = 0$: this case corresponds, for example, to decays into two $J = 0$ particles, as in the decays of $a_2(1320)$ and $a_2(1700)$ to $\eta\pi$ or $\mathrm{K\overline{K}}$ [5].

Because of the symmetry of these conditions by exchange of final and initial state, as mentioned above, the same blue contours also refer to the joint requirement that the particle is produced alone from the scattering of two real gluons (suppression of $M = \pm 1$, in the CS frame) and decays into two $J = 1/2$ fermions, so that $\sigma_{\pm 1}^{G'} = \sigma_M^{\pm 2} = 0$.

The orange areas describe the case of a decay to a final state having always $J_{z'}$ projection $G' = \pm 1$. This happens, for example, if the daughters are a $J = 0$ particle and a photon, as in the decay $a_2(1320) \to \pi^{\pm}\gamma$ [5].

Figure 7.6 shows the shapes assumed by the angular distribution for the different combinations of initial and final state angular momentum projections, in the parity-conserving case ($\lambda_1 = \lambda_3 = 0$). Only the examples with $|G'| \leq |M|$ are drawn: the remaining ones are related to these through the above-mentioned symmetry by exchange of M with G'.

Parity violation is possible in three out of the six distinct cases shown in Fig. 7.6. The parity asymmetry is parametrized by the amplitude combinations β_{11}, β_{12} and β_{22} in Eq. 7.23: whenever the initial or final state have zero J_z or J'_z projections, λ_1 and λ_3 vanish. The corresponding distributions are shown in Fig. 7.7 for the two maximal and opposite asymmetry effects.

The anisotropy parameters corresponding to the shapes shown in Figs. 7.6 and 7.7 are indicated on the $\lambda_2 - \lambda_4$ and $\lambda_1 - \lambda_3$ maps of Fig. 7.8. The Grail-shaped distribution defined by $M = \pm 1, G' = 0$ (or vice-versa) represents the asymptotic vertex of the domain area at $\lambda_2 \to +\infty, \lambda_4 \to -\infty$, where $w(\cos\vartheta) \propto \cos^2\vartheta \sin^2\vartheta$.

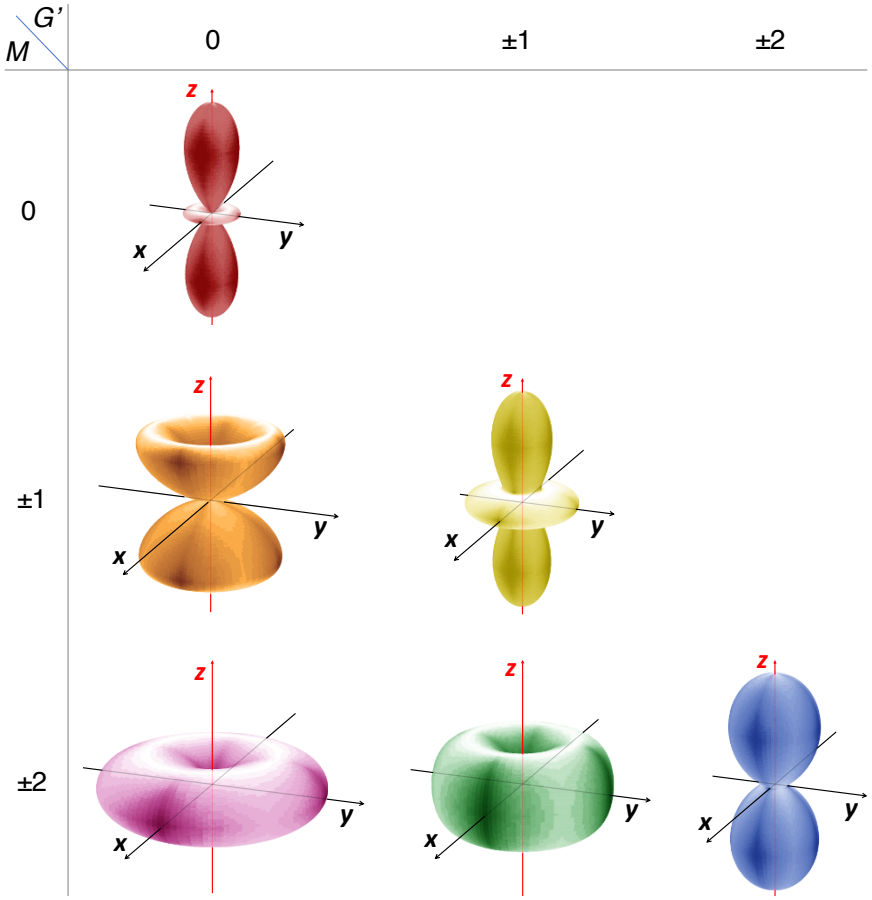

Fig. 7.6 Shapes of the angular distributions of the parity-conserving two-body decay $O \to X_1X_2$ of a $J = 2$ particle, for all combinations of angular momentum projections of O along z (M) and of the X_1X_2 system along z' (G'). Off-diagonal combinations with $|G'| > M$, here omitted, can be obtained by exchanging M with G'.

7.6 Case study: spin characterization of a heavy di-photon resonance

The above-mentioned graviton hypothesis was one of the several models considered as possible interpretations of the "Higgs-like" resonance observed by the ATLAS and CMS experiments [7, 8], before its definitive identification. We will now examine this latter physical example as an illustration of how the determination of the shape of the decay distribution can lead, with minimal assumptions, to the characterization of an unknown particle.

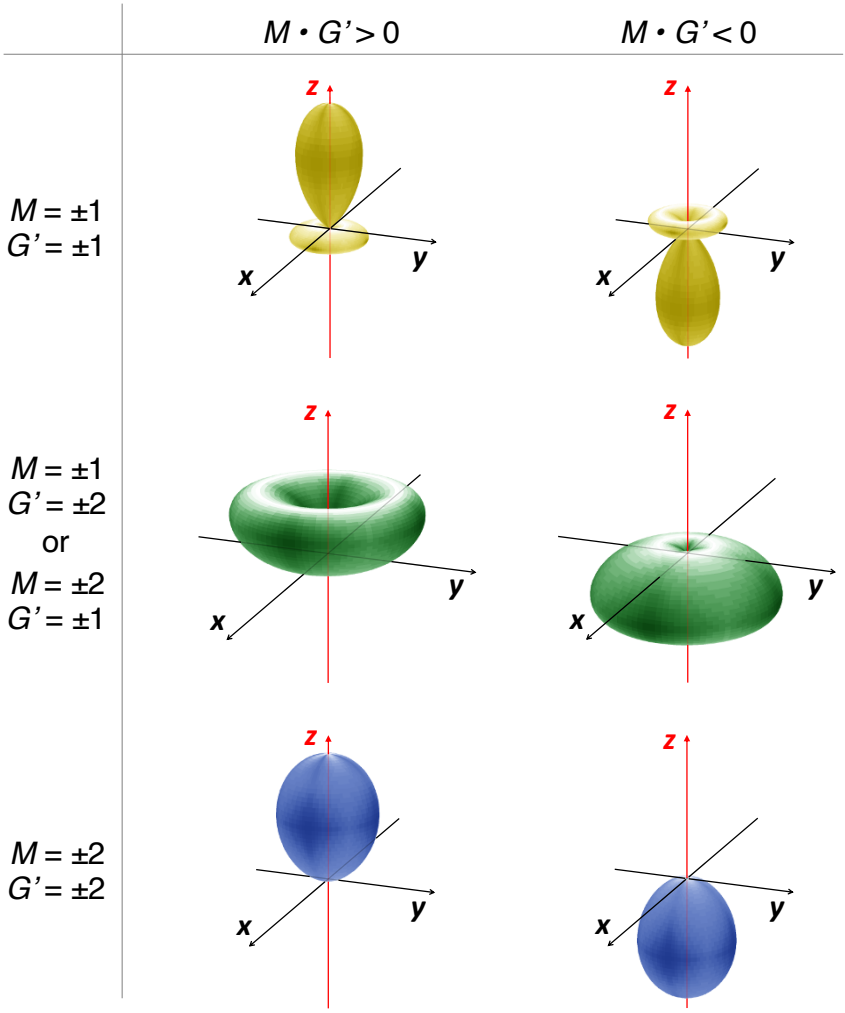

Fig. 7.7 Shapes of the angular distributions of the maximally parity violating two-body decay $O \to X_1X_2$ of a $J = 2$ particle, for the three relevant combinations (rows) of angular momentum projections of O along z (M) and of the X_1X_2 system along z' (G'), and for the two opposite signs of the effect (columns).

As a first step in the determination of the angular momentum quantum number of the hypothetical new resonance, it is interesting to note that a particle assumed to be produced with no recoil from the fusion of two real gluons and decaying into two real photons always produces a significant polar anisotropy ($\lambda_i \neq 0$ for some i) with respect to the scattering direction of the gluons, except, obviously, in the $J = 0$ case, corresponding to $\mathrm{H} \to \gamma\gamma$.

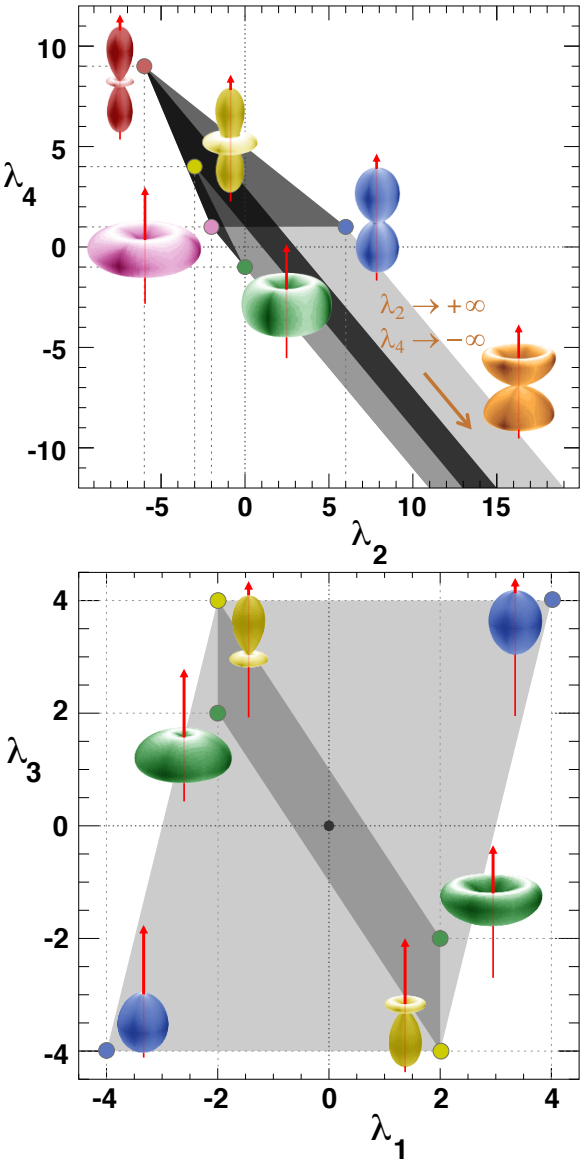

Fig. 7.8 The (λ_2, λ_4) and (λ_1, λ_3) coordinates of the polarization examples shown in Figs. 7.6 and 7.7.

This effect is seen in Fig. 7.4 for the $J = 2$ case, being λ_4 always ≥ 1. It can, moreover, be generalized to other J values. The $J = 1$ case is excluded by the Landau–Yang theorem [9, 10], stating that a $J = 1$ particle cannot decay into two

real (transversely polarized) photons (nor, equivalently, be produced alone by two transversely polarized gluons). Let us consider then $J = 3$ and $J = 4$.

The polar projection of the di-photon decay distribution of a $J = 3$ particle produced by gluon-gluon fusion is described by the parameters

$$\begin{aligned} \lambda_2 &= 3\,(3\,\alpha_{00} + 10\,\alpha_{02} - 5\,\alpha_{22})\,/\,D\,, \\ \lambda_4 &= 10\,(-3\,\alpha_{00} - 6\,\alpha_{02} + \alpha_{22})\,/\,D\,, \\ \lambda_6 &= (25\,\alpha_{00} + 30\,\alpha_{02} + 9\,\alpha_{22})\,/\,D\,, \end{aligned} \tag{7.27}$$

with $D = 4\,\alpha_{22}$ and α_{ij} defined as in Eq. 7.24.

The corresponding $J = 4$ decay parameters are

$$\begin{aligned} \lambda_2 &= 4\,(-45\,\alpha_{00} - 160\,\alpha_{02} + 52\,\alpha_{22})\,/\,D\,, \\ \lambda_4 &= 10\,(111\,\alpha_{00} + 312\,\alpha_{02} - 32\,\alpha_{22})\,/\,D\,, \\ \lambda_6 &= -140\,(15\,\alpha_{00} + 32\,\alpha_{02} + 4\,\alpha_{22})\,/\,D\,, \\ \lambda_8 &= 49\,(25\,\alpha_{00} + 40\,\alpha_{02} + 16\,\alpha_{22})\,/\,D\,, \\ \text{with}\quad D &= 9\,\alpha_{00} + 40\,\alpha_{02} + 16\,\alpha_{22}\,. \end{aligned} \tag{7.28}$$

In both cases the parity-violating λ_i parameters (odd i) vanish. The parameter domains for $J = 2$, 3 and 4 in the CS frame are shown in Fig. 7.9. The minimum distance from the origin ($\lambda_i = 0$ for any i, corresponding to $J = 0$) increases from $J = 2$ to $J = 3$ to $J = 4$ and, in general, should increase with J, reflecting the higher level of relative polarization represented by the limitation of the initial- and final-state helicities to $M = 0, \pm 2$ and $G' = 0, \pm 2$: the larger is the modulus of $\mathbf{J}$, the more of its projections become forbidden (for example, ± 3 in the $J = 3$ case, ± 3 and ± 4 in the $J = 4$ case, etc.).

It is interesting to note that, as shown in Fig. 7.10, the three domains have no intersections between them and also not with the $J = 0$ point ($\lambda_i = 0$ for any i). Therefore, a sufficiently-precise measurement of the di-photon decay distribution can provide an unambiguous spin characterization, independent of further specific hypotheses on the identity of the particle and how it is produced and interacts.

Figure 7.11 illustrates the dependence of the observable $\cos\vartheta$ distribution on J, for the $J = 2$, 3 and 4 cases. The curves were obtained by scanning the (respectively, two-, three- and four-dimensional) physical domains of the λ_i parameters.

A more immediate geometrical illustration of the J dependence of the angular distribution is given by Fig. 7.12, for each of the three allowed combinations of gluon-gluon and photon-photon polarizations: ($M = 0, G' = 0$), ($M = \pm 2, G' = 0$) (or vice-versa), and ($M = \pm 2, G' = \pm 2$). The recognizable shape differences seen in these figures show that it is always possible to unambiguously resolve the value of J between the three options.

The experimental precision needed to achieve a significant discrimination obviously depends on J and on the actual values of the polarization parameters, that is,

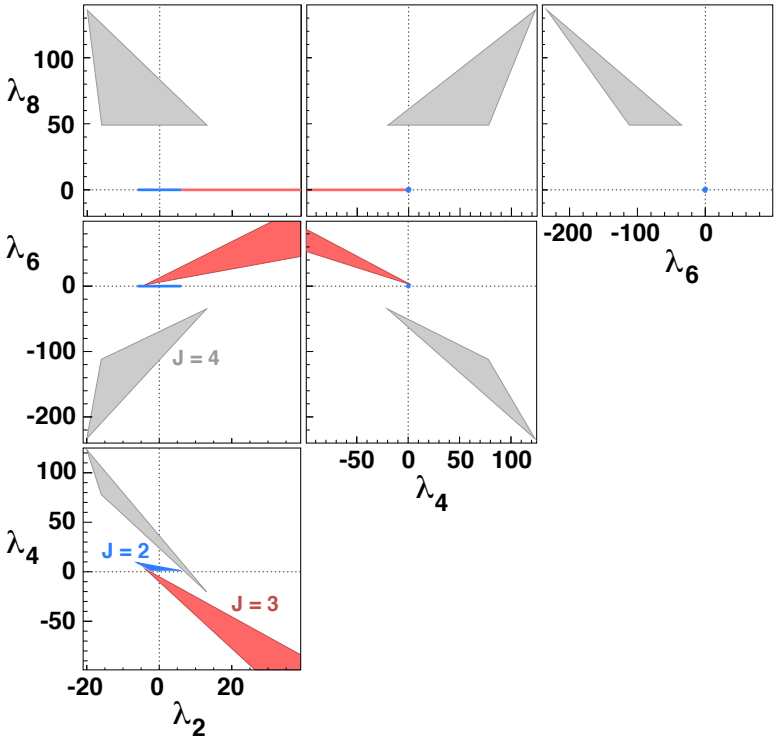

Fig. 7.9 Allowed regions for the polar anisotropy parameters (in the CS frame) of the decay distribution of a particle produced by gluon-gluon fusion and decaying into two photons. The three different shades indicate, from darkest (blue) to lightest (grey), the $J = 2$, 3 and 4 cases. In the $J = 3$ case there are no upper bounds on λ_2 and λ_6 and no lower bound on λ_4.

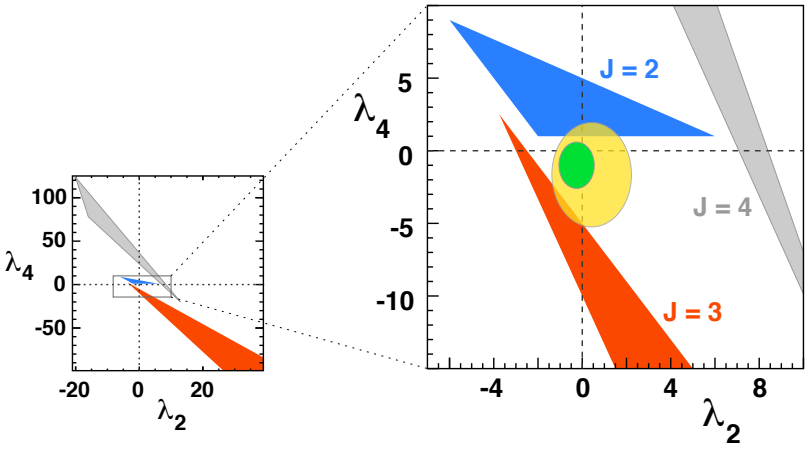

Fig. 7.10 Zoom of the top plot of Fig. 7.9 around the origin, with ellipses representing hypothetical measurements favouring the $J = 0$ hypothesis.

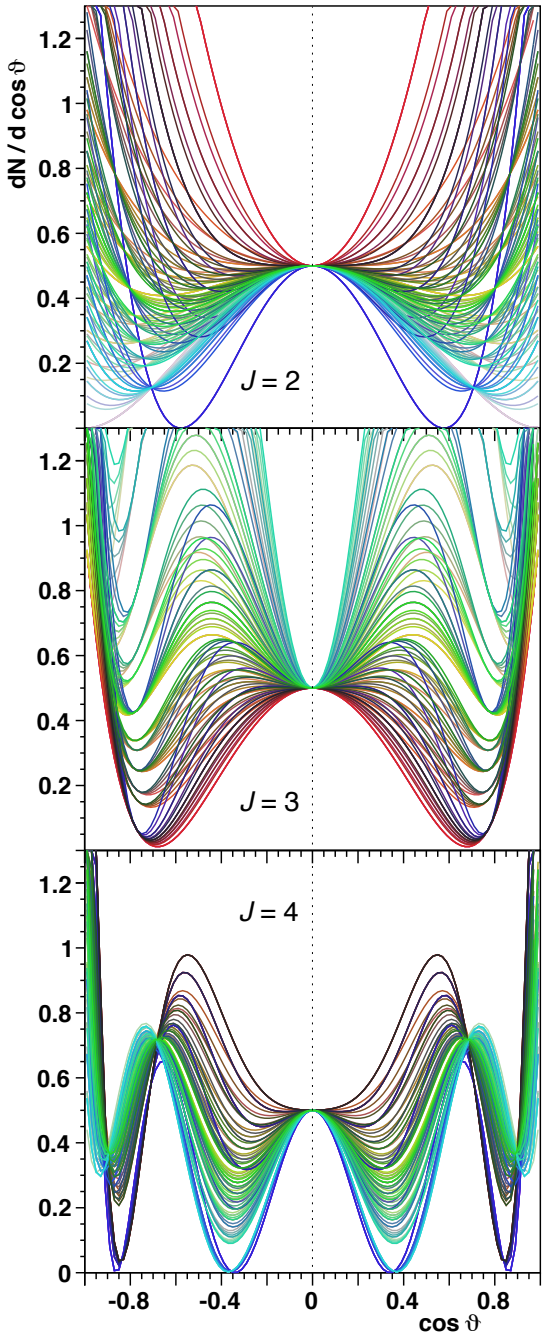

Fig. 7.11 Physically allowed $\cos\vartheta$ distributions in the CS frame for (from top to bottom) $J = 2$, 3 and 4 bosons produced by gluon-gluon fusion and decaying into two photons. For clarity of representation, all distributions are normalized to the same (arbitrary) value at $\cos\vartheta = 0$.

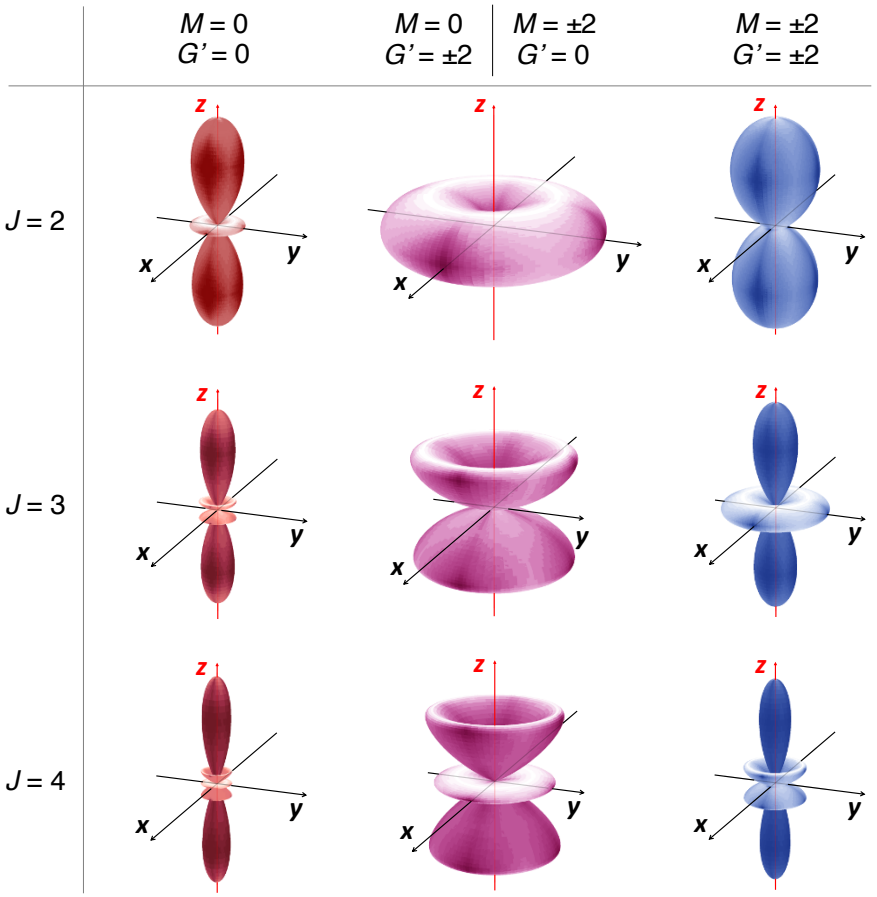

Fig. 7.12 Shapes of the angular distributions for $J = 2$, 3, and 4 bosons produced by gluon-gluon fusion and decaying into two photons, for the three allowed combinations of initial- and final-state polarizations.

on the identity of the particle. Figure 7.10 includes two ellipses representing putative measurements of different uncertainties. Both include the origin $\lambda_2 = \lambda_4 = 0$, which corresponds to the isotropic distribution that only a $J = 0$ particle can yield if produced by gluon-gluon fusion. The larger experimental contour excludes the $\lambda_2 = 6$, $\lambda_4 = 1$ point, eliminating the hypothesis that the decaying boson is a graviton-like $J = 2$ particle of the kind mentioned above. However, it does not rule out hypothetical $J = 2$ (or even $J = 3$) boson identities corresponding to the smallest values that λ_2 and λ_4 can have for those angular momentum values. The inner ellipse illustrates another hypothetical measurement, sufficiently precise to exclude the full $J = 2$ and $J = 3$ domains, thereby leading to the model-independent spin characterization of a $J = 0$ particle.

7.7 Decay distributions of half-integer spin particles

Expanding Eq. 7.12 for $J = 1/2$, we find that the most general distribution is

$$\begin{aligned} W(\cos\vartheta, \varphi) \;=\; \frac{1}{4\pi}\,(1 &+ \nu_\vartheta \cos\vartheta \\ &+ \nu_\varphi \sin\vartheta\cos\varphi \\ &+ \nu_\varphi^\perp \sin\vartheta\sin\varphi)\,, \end{aligned} \tag{7.29}$$

with

$$\begin{aligned} \nu_\vartheta &= \frac{1}{D}\left(\rho^{+\frac{1}{2}}_{+\frac{1}{2},+\frac{1}{2}} - \rho^{-\frac{1}{2}}_{+\frac{1}{2},+\frac{1}{2}} + \rho^{-\frac{1}{2}}_{-\frac{1}{2},-\frac{1}{2}} - \rho^{+\frac{1}{2}}_{-\frac{1}{2},-\frac{1}{2}}\right) \\ \nu_\varphi &= \frac{2}{D}\,\mathrm{Re}\left(\rho^{+\frac{1}{2}}_{+\frac{1}{2},-\frac{1}{2}} - \rho^{-\frac{1}{2}}_{+\frac{1}{2},-\frac{1}{2}}\right), \\ \nu_\varphi^\perp &= \frac{2}{D}\,\mathrm{Im}\left(\rho^{+\frac{1}{2}}_{+\frac{1}{2},-\frac{1}{2}} - \rho^{-\frac{1}{2}}_{+\frac{1}{2},-\frac{1}{2}}\right), \\ \text{where}\;\; D &= \rho^{+\frac{1}{2}}_{+\frac{1}{2},+\frac{1}{2}} + \rho^{-\frac{1}{2}}_{-\frac{1}{2},-\frac{1}{2}} + \rho^{-\frac{1}{2}}_{+\frac{1}{2},+\frac{1}{2}} + \rho^{+\frac{1}{2}}_{-\frac{1}{2},-\frac{1}{2}}\,. \end{aligned} \tag{7.30}$$

The three parameters measure differences between yields characterized by a given spin orientation of the final state and those with the opposite spin orientation, with respect to a given initial state configuration. They clearly represent parity asymmetries. In fact only parity-violating decays show anisotropic decay distributions. This is the case, for example, of the decays of the top quark into a W boson and a b quark, and of the Λ hyperon into a proton and a pion.

The decay anisotropy due to parity violation is measurable only if the particle is also produced polarized, with its spin preferentially aligned along a certain "positive" or "negative" direction in the chosen polarization frame; if this does not happen, the decay angles cannot be referred to a reference direction maintaining consistent orientation event after event and the corresponding parity violation becomes unobservable. In fact, each anisotropy parameter can be thought as the product of two parameters, one expressing the polarization induced by the production mechanism, the other being the parity-violating asymmetry of the decay, and it is nonzero only when both are.

For example, the top quark seemingly decays almost isotropically in $t\bar{t}$ production [11, 12], because of lack of the polarization of the corresponding QCD production mechanism; however, its intrinsic left-handed nature is revealed with significant decay anisotropies in single-t events [13], where it is produced polarized.

The polarization of the Λ is an exception to the rule that the natural polarization axis tends to stay, at least on average, inside the production plane. In fact, since the mid-1970's fixed-target experiments have been showing [14] that the polariza-

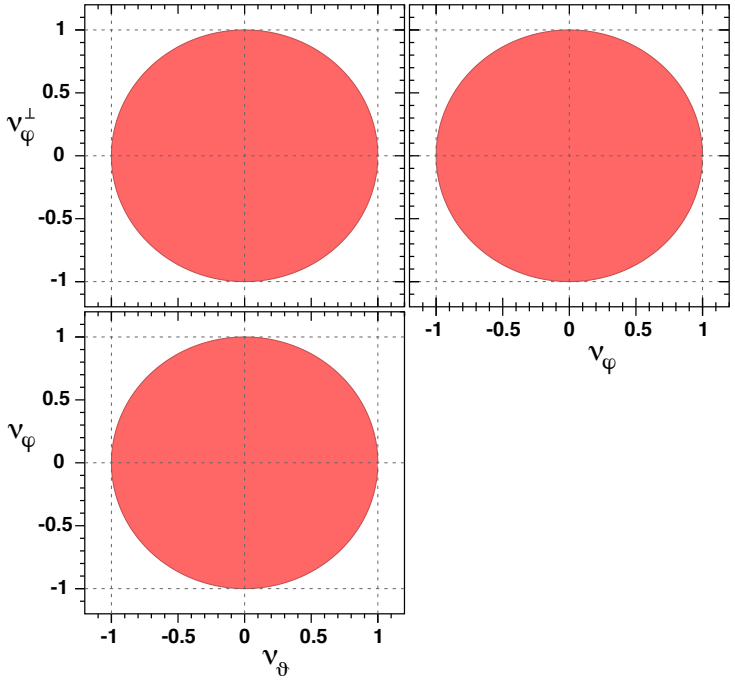

Fig. 7.13 Allowed parameter regions of the two-body decay distribution of a $J = 1/2$ particle.

tion is largest along a quantization axis *perpendicular* to the production plane. The implications of this unexpected observation on the underlying QCD mechanisms, which must confer a polarization to the s quark, have been the subject of several experimental and theoretical studies [15], but the question is still open. It remains true that in symmetric collisions and in the limit of zero longitudinal momentum (x_F or y) the anisotropy along such axis vanishes, as confirmed by the small polarization measured by the ALICE experiment at the LHC [16].

The physically allowed domain of the ν parameters, shown in Fig. 7.13 in its three projections, is simply a sphere defined by the relation

$$\tilde{\nu} = \sqrt{\nu_\vartheta^2 + \nu_\varphi^2 + \nu_\varphi^{\perp 2}} \leq 1 \,. \tag{7.31}$$

It is easy to recognize that, under a generic rotation of the polarization frame $R_z(\omega)\, R_y(\zeta)\, R_z(\psi)$ (see Section 2.15), the parameters ν_ϑ, ν_φ, and $\nu_\varphi^\perp$ simply transform according to the same rotation as the vector (z, x, y):

$$\begin{pmatrix} \nu'_\vartheta \\ \nu'_\varphi \\ \nu_\varphi^{\perp\prime} \end{pmatrix} = \begin{pmatrix} \cos\zeta & \sin\zeta\cos\psi & \sin\zeta\sin\psi \\ -\sin\zeta\cos\omega & \cos\zeta\cos\omega\cos\psi - \sin\omega\sin\psi & \cos\zeta\cos\omega\sin\psi + \sin\omega\cos\psi \\ \sin\zeta\sin\omega & -\cos\zeta\sin\omega\cos\psi - \cos\omega\sin\psi & -\cos\zeta\sin\omega\sin\psi + \cos\omega\cos\psi \end{pmatrix} \begin{pmatrix} \nu_\vartheta \\ \nu_\varphi \\ \nu_\varphi^\perp \end{pmatrix} .$$

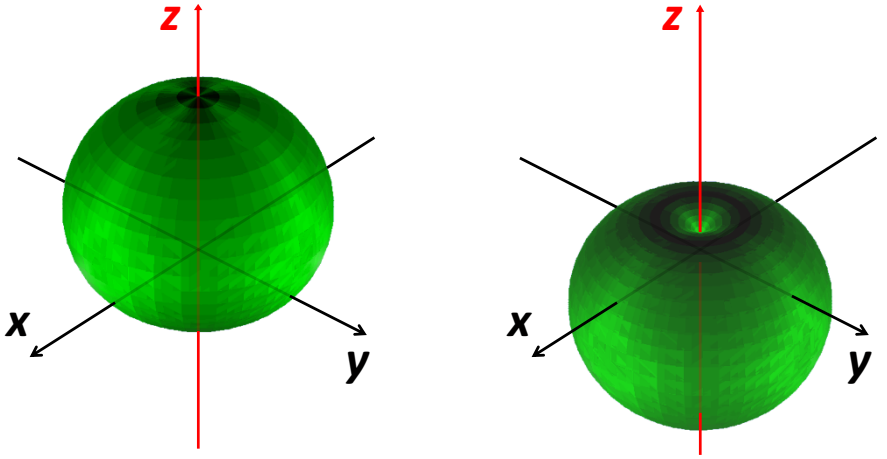

Fig. 7.14 Shape of the decay distribution of a $J = 1/2$ particle produced fully polarized and decaying with maximum parity asymmetry along the chosen z axis, when the initial and final states have same-sign (left) or opposite-sign (right) projections M and G'.

The rotation preserves $\tilde{\nu}$, which, therefore, represents the maximum measurable value of the asymmetry ν_ϑ along any chosen reference axis z and is obviously invariant for any frame transformation, while ν_ϑ, ν_φ and $\nu_\varphi^\perp$ are themselves invariant by rotations around, respectively, the z, x and y axes.

Another way of expressing these considerations on the rotational property of the distribution is that the three angular expressions $\cos\vartheta$, $\sin\vartheta\cos\varphi$ and $\sin\vartheta\sin\varphi$ entering Eq. 7.29 are equal, respectively, to the direction cosines $\cos\theta_z$, $\cos\theta_x$ and $\cos\theta_y$. It is an option for the experimental analysis to consider, in fact, the three one-dimensional distributions of these variables, which have the form $w(\cos\theta_z) \propto 1 + \nu_\vartheta \cos\theta_z$, etc., and yield the three parameters ν_ϑ, ν_φ and $\nu_\varphi^\perp$ individually, even if with statistical correlations more difficult to be accounted for, since the number of independent angular degrees of freedom remains only two.

Figure 7.14 shows the shape of the distribution in the extreme cases when the production and decay asymmetries are (for best visualization) maximum along the chosen axis, that is, $w(\cos\vartheta) = \frac{1}{2}(1 \pm \cos\vartheta)$.

We finally report the expressions for the polar anisotropy parameters of the decay of a $J = 3/2$ particle:

$$\begin{aligned}
\lambda_1 &= \left(-5\beta_{\frac{1}{2}\frac{1}{2}} + 3\beta_{\frac{3}{2}\frac{3}{2}} + 6\beta_{\frac{1}{2}\frac{3}{2}}\right)/D\,,\\
\lambda_2 &= \left(3\alpha_{\frac{1}{2}\frac{1}{2}} + 3\alpha_{\frac{3}{2}\frac{3}{2}} - 6\alpha_{\frac{1}{2}\frac{3}{2}}\right)/D\,,\\
\lambda_3 &= \left(9\beta_{\frac{1}{2}\frac{1}{2}} + \beta_{\frac{3}{2}\frac{3}{2}} - 6\beta_{\frac{1}{2}\frac{3}{2}}\right)/D\,,\\
\text{with}\quad D &= \alpha_{\frac{1}{2}\frac{1}{2}} + \alpha_{\frac{3}{2}\frac{3}{2}} + 6\alpha_{\frac{1}{2}\frac{3}{2}}\,,
\end{aligned} \tag{7.32}$$

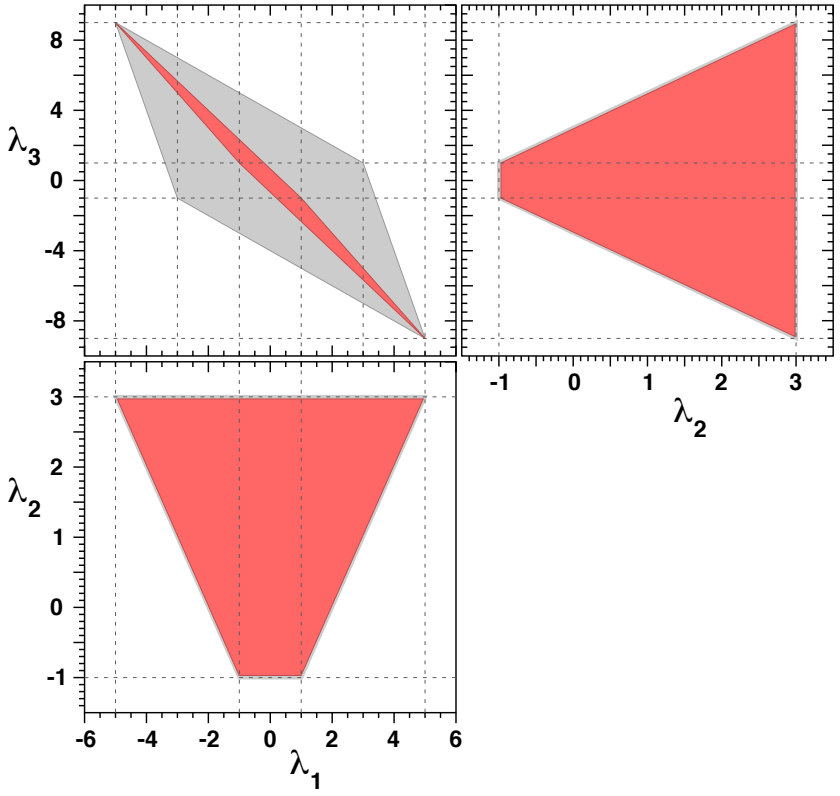

Fig. 7.15 Allowed parameter regions for the polar anisotropy parameters of the two-body decay distribution of a $J = 3/2$ particle. The largest areas (grey) represent the most general domain while the inner areas (red) represent the case of the decay into a system having G' projection $\pm 1/2$, as in the proton–pion and proton–kaon channels.

where α_{ij} and β_{ij} are the parity-conserving and parity-violating amplitude combinations defined in Eq. 7.24. The most general domain of these parameters is represented by the grey areas in Fig. 7.15, while the smaller red areas refer to the decay where $G' = \pm 1/2$, corresponding for example to the decays of the $J = 3/2$ N, Δ, and Λ baryons into proton–pion and proton–kaon, and of the Ω to Λ–kaon [5].

While the decay of a $J = 1/2$ particle is always isotropic in the absence of parity-violating effects, this is not true for the $J = 3/2$ case, where the angular distribution in the parity-conserving case has the form $\propto 1 + \lambda_2 \cos^2 \vartheta$, with λ_2 included between -1 and $+3$.

The shapes assumed by the distribution for all combinations of natural polarizations of the initial state (along z) and of the final state (along z') are shown in Fig. 7.16. The first two columns refer to the maximally parity-violating cases where initial- and final- state helicities have, respectively, always the same or always opposite signs, while the third column shows the parity-conserving distributions where

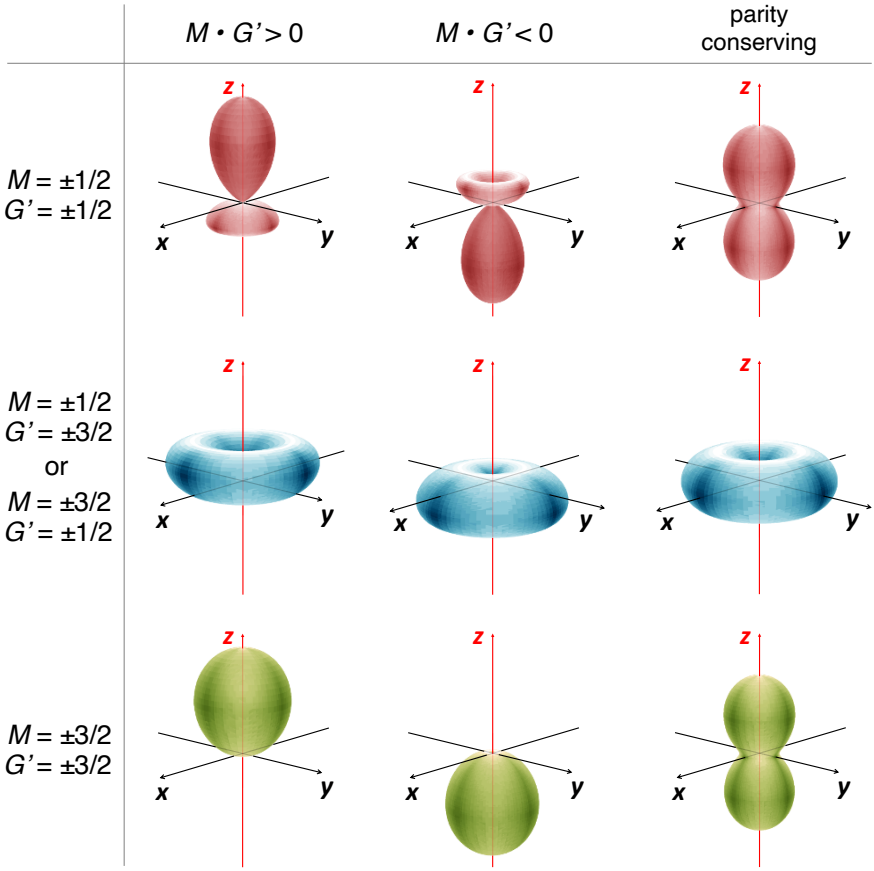

Fig. 7.16 Shape of the angular distribution produced by a $J = 3/2$ particle in a pure J_z state (M) decaying into a two-body system being a pure $J_{z'}$ state (G'); the colums represent, respectively, the two maximally and oppositely parity-violating cases and the parity-conserving case.

the signs of the helicities are uncorrelated. The $(\lambda_1, \lambda_2, \lambda_3)$ values corresponding to these shapes are shown in Fig. 7.17.

7.8 When "polarized" and "anisotropic" are seemingly not equivalent

After seeing expressions of the angular distribution parameters for generic decay channels, we can discuss the relation between the concepts of "particle polarization" and "decay anisotropy" in a more complete way, with respect to what was possible by examining the dilepton decay case in the previous chapters. Referring

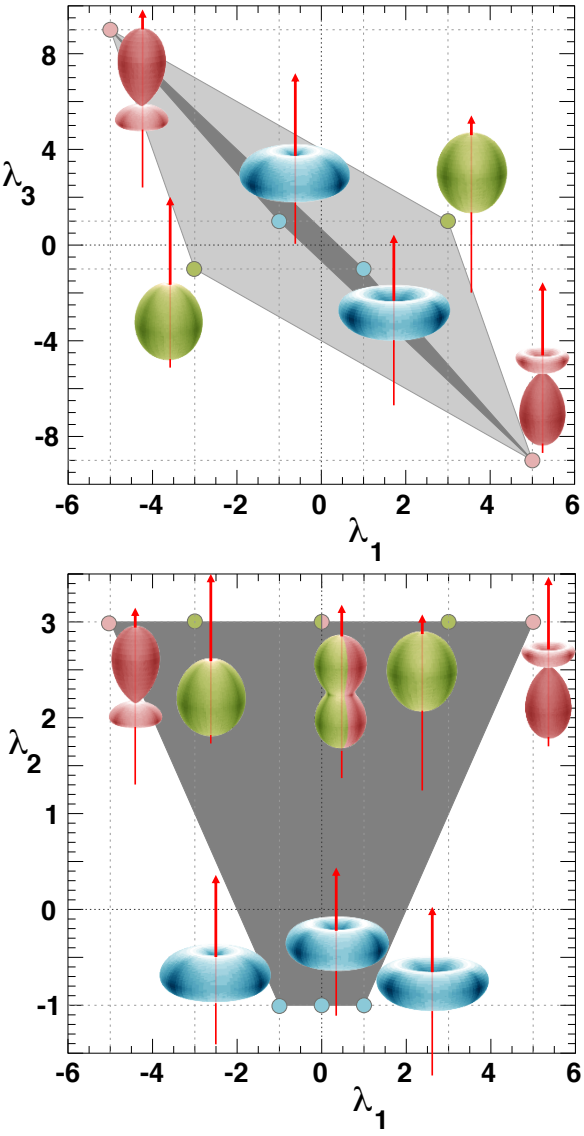

Fig. 7.17 The shape-parameter values of the polarization examples shown in Fig. 7.16.

in particular to the $J = 1$ case (Eq. 7.19), we now see a general feature: even considering one individual production process, where the particle is fully polarized, for example in the (longitudinal) $J_z = 0$ state (that is, the matrix elements $\rho^{G'}_{0,0}$ are the only nonzero ones), if the final state can have $G' = -1$, 0, or $+1$ with identical probabilities ($\rho^{-1}_{0,0} = \rho^{0}_{0,0} = \rho^{+1}_{0,0}$), then the distribution appears to be isotropic. The same result can be seen for any other angular momentum configuration of the initial

particle, being, for example, λ_ϑ a sum of terms of the kind $\rho^{+1}_{M,M} + \rho^{-1}_{M,M} - 2\rho^{0}_{M,M}$. In other words and more generally, the polarization of the decaying particle is observable through a measurable anisotropy of its two-body decay distribution only if also the *final* state is "polarized", being a superposition of $J_{z'}$ eigenstates with unequal weights. This is a completely general condition, satisfied, for example, also by the expressions of the polar anisotropy parameters of the distribution for a $J = 2$ particle (Eq. 7.23): all λ_i coefficients can be seen to vanish when it is imposed that $\sigma^j_i = \sigma^k_i$ for any i, j, and k. As we already mentioned in Section 7.7, each anisotropy parameter of the $J = 1/2$ decay reflects the product of initial state polarization and partity-violating decay asymmetry.

It remains true that a $J = 1$ particle is always produced intrinsically polarized, in the sense defined by Theorem 1.1, presented in Section 1.10: in every individual event it has always angular projection $M = \pm 1$ along some direction. As we have seen in Chapters 5 and 6, smearing effects, happening when that direction changes event after event with respect to the chosen reference frame, can attenuate or even completely hide the natural polarization. Assuming that none of such effects is at play here, there is a general condition for the observability of the polarization of a particle in its two-body decay: the final state must have a non-uniform pattern of spin orientations G', effectively providing the "analyzing power" of the decay. This is what usually happens, as seen in the examples considered, thanks to either the coupling properties of the involved particles (as helicity conservation in the dilepton decay) or simply because of angular momentum conservation, which often forbids certain $J_{z'}$ configurations of the final state.

Concerning the latter case, we have seen, in the previous sections, examples where the polarization becomes observable because $J_1 + J_2 < J$. Another possibility is that one of the decay particles has a definite polarization, as in the case of the transverse photon.

This fact is well illustrated by the already noticed difference between the angular distributions of the decays $\chi_{cJ} \to \mathrm{J}/\psi\,\gamma$ and $\chi_{cJ} \to \mathrm{J}/\psi\,\gamma^*$. In the first decay the emitted photon is real and transverse. Its $J_{z'}$ projection (Fig. 6.32), which can only be ± 1, rules out, because of angular momentum conservation, certain $J_{z'}$ projections of the J/ψ, which is, therefore, polarized. Above all, the J/$\psi\,\gamma$ system is polarized, that is, the values of its total $J_{z'}$ projection, $G' = L' + K' = -J, \ldots, +J$, are not equally probable, leading, as seen in Sections 7.4 (χ_{c1}) and 7.5 (χ_{c2}), to anisotropic χ_c decay distributions with shapes univocally correlated to the polarization.

When, instead, the photon is virtual, there is no constraint on its polarization and these $J \to (J = 1) + (J = 1)$ transitions become a "natural" illustration of the angular momentum addition rule $J = 1 \oplus 1$, where all possible G' combinations of the decay system compatible with $|G'| \leq J$ participate with equal weights, without any restriction imposed by the physical interaction driving the decay. This "unpolarized" final state does not provide any analyzing power for the determination of the mother particle's polarization. The J/ψ is, hence, emitted isotropically in the χ_c polarization frame, leading to the seemingly paradoxical case where the measurement of the two-body decay angular distribution is blind to the polarization state of the decaying particle.

The solution of the paradox is that this conclusion is true only when the measurement ignores the information contained in the subsequent decays of the final-state particles. A suitable analysis of the shapes of their own decay angular distributions *will* provide the necessary analyzing power.

The full information on the χ_c polarization state remains available in the higher-dimensional distribution of the cascade process $\chi_{cJ} \to \mathrm{J}/\psi\,\gamma^*$, $\mathrm{J}/\psi \to \ell^+\ell^-$, $\gamma^* \to \ell^+\ell^-$, determinable either in the frame (cHX) defined in Fig. 6.1 or in the one (CC) defined with the alternative J/ψ polarization axes of Fig. 6.3. Exploiting the full dimensionality of the process with its underlying variable correlations is always beneficial, also from the experimental point of view, since it minimizes the risks of analysis biases, presented by the blind integration over physical degrees of freedom (as we have seen in Section 2.13). In this case, however, as seen in Section 6.8, with the choice of the CC frame the anisotropy of the J/ψ dilepton decay alone, after integration over the angles of the χ_c decay, is fully sensitive to the χ_c polarization. Moreover, with the same axis definition, the dilepton distribution produced by the virtual photon is identical to the J/ψ one and carries a further "duplicate" of the χ_c polarization information.

7.9 Recapitulation

In the calculation of a decay angular distribution, the functional dependence on the decay angles is determined by the elements of the Wigner matrix, $\mathcal{D}^J_{LL'}$, corresponding to the total angular momentum J of the decaying particle O. In the considered case of a two-body decay, the matrix transforms the angular momentum projection (L') of the final state, as defined along the common direction, z', of the decay products X_1 and X_2 in the O rest frame, into the projection (L) on the quantization axis z chosen for O (Fig. 7.1-right), allowing us to impose the conservation $J_z(X_1 + X_2) = J_z(O)$. Section 7.1 describes the Wigner matrices in a form suitable for these calculations, which depends on the two spherical angles ϑ and φ defining the relative orientations of z' and z. The dependence is factorized as $\mathcal{D}^J_{LL'}(\vartheta,\varphi) = \exp[-i(L-L')\,\varphi]\; d^J_{LL'}(\vartheta)$, with the "reduced" elements $d^J_{LL'}(\vartheta)$ defined in Eq. 7.3. Explicit analytical expressions of the reduced matrix elements for J between $1/2$ and 4 are given in Tables 7.1–7.6.

The decay amplitude is a linear combination of Wigner matrix elements (Eqs. 7.6 and 7.7); the coefficients, $\mathcal{A}_{M,G'_1,G'_2}$, are complex amplitudes representing the dynamics of both the production and the decay of O (Fig. 7.1-left). In fact they express, on one hand, the probability of a given J_z projection, M, of O, that is, the polarization that O inherited in the production process. On the other hand, they reflect the properties of the final states X_1 and X_2, as well as of their coupling to O, by representing the probabilities of their possible $J_{z'}$ projections, G'_1 and G'_2.

The general expression of the angular distribution, squared modulus of the amplitude (Eq. 7.12), depends linearly on the "spin" density matrix elements $\rho^{G'}_{M,M}$, defined in Eq. 7.13 as the sum of all relevant products between an amplitude and a

complex-conjugate amplitude, also averaged over all possible contributing mechanisms.

The polar projection of the distribution (Eq. 7.15), depending only on the diagonal (and real) density matrix elements $\sigma_M^{G'} \equiv \rho_{M,M}^{G'}$ (Eq. 7.16), is a polynomial of order $2J$ in $\cos\vartheta$ and its $2J$ observable parameters are certainly much easier to handle in a measurement than those of the full distribution, which, for example, for $J = 2$ are 24 instead of 4.

The most general decay distribution of a $J = 1$ particle into any two-body final state (Eq. 7.18) is formally the same as for the dilepton decay of a vector particle (Eq. 1.29), depending on eight observable parameters, three of which parity-violating and two more vanishing in inclusive observations. The difference is in the dependence on the amplitudes (Eq. 7.19): the dilepton (helicity-conserving) case (Eq. 1.28) corresponds to setting the density matrix elements $\rho_{M,M}^0$ to zero. The allowed parameter space is, therefore, different (Fig. 7.2). For a given initial particle and polarization (M), the angular distributions of the decays into dilepton and into, for example, two $J = 0$ particles are as different as they could be, as shown by the comparison made in Fig. 7.3, which applies, for example, to the decays $\Upsilon(4S) \to B\overline{B}$ and $\Upsilon(4S) \to \ell^+\ell^-$.

Further examples of how the distribution changes for different final state particles and, also, for different production channels (which determine different possible polarizations of O) are given in Section 7.5 for the $J = 2$ case, considering, for simplicity, only the polar component, that is, the pure J_z eigenstates of the decaying particle (Fig. 7.6), and maximal parity violation effects (Fig. 7.7). Section 7.6 illustrates, with an example, how the identity of the production and decay channels strongly constrains the allowed shapes of the decay distributions. In particular, an unidentified particle produced by gluon-gluon fusion and decaying into two photons can be characterized with a measurement of its decay distribution without the need of injecting further theoretical hypotheses on it production mechanism. The allowed physical domains of the $J = 0$, 2, 3, and 4 cases ($J = 1$ being excluded by the Landau–Yang theorem) are disjointed from one another and can be experimentally discriminated (Fig. 7.10). In fact, the shapes of the distributions have characteristic differences, essentially in the number of changes of sign of the derivative of the $\cos\vartheta$ distribution (Fig 7.11), that is, in the number of "lobes" of the three-dimensional shape (Fig. 7.12). Clearly, more specific hypotheses, completely fixing the polarization of the produced particle, can be tested and rejected with higher significance, since they correspond to one point, instead of a region, in the parameter domain and to *one* of the possible curves or shapes seen in those figures.

The decays of half-integer spin particles are briefly illustrated in Section 7.7. In particular, in the $J = 1/2$ case the $\cos\vartheta, \varphi$ distribution (Eq. 7.29) is either isotropic or parity-violating, that is, its three parameters are asymmetries (Eq. 7.30), vanishing when either the production mechanism or the decay are parity-conserving. Instead, for the $J = 3/2$ distribution, parity-conserving but strongly anisotropic physical cases exist, where it assumes the form $1 + \lambda_2 \cos^2\vartheta$, with $\lambda_2 = -1$ for $|M| = 1/2$ and $|G'| = 3/2$, or vice-versa, and $\lambda_2 = +3$ for $|M| = |G'| = 3/2$ or $1/2$ (Figs. 7.16 and 7.17).

We saw in the previous chapter that an intrinsically polarized vector particle can appear as unpolarized if it is produced in the decay of a $J = 0$ state and the existence of this first decay step is ignored in the analysis. The natural polarization of the vector particle can, however, at least in principle, be measured, by reconstructing the two-step decay chain in its full dimensionality. In this chapter we have provided a further example of how an isotropic decay distribution can be observed even if the particle is naturally polarized.

A common feature recognizable in all formulas expressing the shape parameters of the two-body decay distribution as functions of the spin density matrix elements is that, for any J, a fully isotropic distribution is obtained not only when O is produced as an identical mixture of $J_z = -J, \ldots, +J$ states, but also (alternatively) when all $J_{z'}$ projections of the system of the decay products are equally probable. In other words, even if the decaying particle is polarized, the resulting two-body angular distribution will appear as isotropic if the final state is "unpolarized", and the polarization of O will seemingly be unobservable. This is a fairly rare occurrence, since the presence of leptons, real photons or $J = 0$ particles in the final state is generally sufficient to provide the $X_1 + X_2$ system with its required "polarization".

As concrete example we considered the decays $\chi_{cJ} \to \mathrm{J}/\psi\,\gamma^*$, where a measurement of the J/ψ emission angles in the χ_{cJ} rest frame always yields an isotropic result, irrespectively of the χ_{cJ} polarization. As in the case of the cascade decay from a $J = 0$ particle, it is actually always possible to perform an experiment that will determine the particle's polarization, by recovering neglected dimensions in the problem. In this case, such dimensions are those of the *subsequent* step in the decay: the angular analysis of the decays of X_1 and X_2, considering correlations with the $O \to X_1X_2$ distribution, will necessarily reveal the polarization of O, provided that X_1 and/or X_2 decay into "polarized" final states. This is the case of the considered example, where the J/ψ and γ^* produce lepton pairs having angular momentum projections ± 1 along their own directions in the J/ψ and γ^* rest frames, because of helicity conservation. Otherwise, the analysis of the cascade should, hypothetically, be further extended to subsequent decay steps.

References

[1] E. P. Wigner, "Group theory and its application to the quantum mechanics of atomic spectra". Pure and applied physics. Academic Press, New York, USA, 1959. ISBN 0127505504.

[2] D. M. Brink and G. R. Satchler, "Angular momentum". Oxford science publications. Clarendon Press, third edition, 1993. ISBN 0198517599.

[3] M. E. Rose, "Elementary theory of angular momentum". Wiley, New York, USA, 1957. ISBN 9780471735243.

[4] E. U. Condon and G. H. Shortley, "The theory of atomic spectra". Cambridge University Press, Cambridge, United Kingdom, 1951. ISBN 9780521092098.

[5] Particle Data Group Collaboration, "Review of Particle Physics", *PTEP* **2020** (2020) 083C01, doi:10.1093/ptep/ptaa104.

[6] Y. Gao et al., "Spin determination of single-produced resonances at hadron colliders", *Phys. Rev. D* **81** (2010) 075022, doi:10.1103/PhysRevD.81.075022, arXiv:1001.3396.

[7] ATLAS Collaboration, "Observation of a new particle in the search for the Standard Model Higgs boson with the ATLAS detector at the LHC", *Phys. Lett. B* **716** (2012) 1, doi:10.1016/j.physletb.2012.08.020, arXiv:1207.7214.

[8] CMS Collaboration, "Observation of a new boson at a mass of 125 GeV with the CMS experiment at the LHC", *Phys. Lett. B* **716** (2012) 30, doi:10.1016/j.physletb.2012.08.021, arXiv:1207.7235.

[9] L. D. Landau, "On the angular momentum of a system of two photons", *Dokl. Akad. Nauk SSSR* **60** (1948) 207, doi:10.1016/B978-0-08-010586-4.50070-5.

[10] C.-N. Yang, "Selection rules for the dematerialization of a particle into two photons", *Phys. Rev.* **77** (1950) 242, doi:10.1103/PhysRev.77.242.

[11] ATLAS Collaboration, "Measurement of top quark polarization in top-antitop events from proton-proton collisions at $\sqrt{s} = 7$ TeV using the ATLAS detector", *Phys. Rev. Lett.* **111** (2013) 232002, doi:10.1103/PhysRevLett.111.232002, arXiv:1307.6511.

[12] CMS Collaboration, "Measurements of $t\bar{t}$ spin correlations and top quark polarization using dilepton final states in pp collisions at $\sqrt{s} = 8$ TeV", *Phys. Rev. D* **93** (2016) 052007, doi:10.1103/PhysRevD.93.052007, arXiv:1601.01107.

[13] CMS Collaboration, "Measurement of top quark polarisation in t-channel single top quark production", *JHEP* **04** (2016) 073, doi:10.1007/JHEP04(2016)073, arXiv:1511.02138.

[14] G. Bunce et al., "Λ^0 hyperon polarization in inclusive production by 300 GeV protons on beryllium", *Phys. Rev. Lett.* **36** (1976) 1113, doi:10.1103/PhysRevLett.36.1113.

[15] A. D. Panagiotou, "Λ^0 polarization in hadron-nucleon, hadron-nucleus and nucleus-nucleus interactions", *Int. J. Mod. Phys. A* **5** (1990) 1197, doi:10.1142/S0217751X90000568.

[16] ALICE Collaboration, "Global polarization of $\Lambda\bar{\Lambda}$ hyperons in Pb-Pb collisions at $\sqrt{s_{NN}}$ = 2.76 and 5.02 TeV", *Phys. Rev. C* **101** (2020) 044611, doi:10.1103/PhysRevC.101.044611, arXiv:1909.01281.